Electrochemical Energy Reviews (2019) 2:574–605
https://doi.org/10.1007/s41918-019-00048-0

REVIEW ARTICLE

Solid-State Electrolytes for Lithium-Ion Batteries: Fundamentals, Challenges and Perspectives

Wenjia Zhao[4] · Jin Yi[2] · Ping He[1] · Haoshen Zhou[1,3]

Received: 11 January 2019 / Revised: 16 April 2019 / Accepted: 1 July 2019 / Published online: 12 August 2019

Abstract
With the rapid popularization and development of lithium-ion batteries, associated safety issues caused by the use of flammable organic electrolytes have drawn increasing attention. To address this, solid-state electrolytes have become the focus of research for both scientific and industrial communities due to high safety and energy density. Despite these promising prospects, however, solid-state electrolytes face several formidable obstacles that hinder commercialization, including insufficient lithium-ion conduction and surge transfer impedance at the interface between solid-state electrolytes and electrodes. Based on this, this review will provide an introduction into typical lithium-ion conductors involving inorganic, organic and inorganic–organic hybrid electrolytes as well as the mechanisms of lithium-ion conduction and corresponding factors affecting performance. Furthermore, this review will comprehensively discuss emerging and advanced characterization techniques and propose underlying strategies to enhance ionic conduction along with future development trends.

Keywords Solid-state electrolyte · Lithium-ion transport · Structure tuning · Interface engineering

1 Introduction

The large-scale application of electric vehicles (EVs) is considered to be a viable method to reduce CO_2 emissions and alleviate greenhouse effects, and in the past few years, the use of EVs has become more accepted by the general public. However, with the rapid adoption of EVs, safety issues as well as other associated issues in the use of lithium-ion batteries (LIBs) as a power source are becoming more pronounced and will require further research and development [1–3]. In general, a commercial LIB is composed of an anode, a non-aqueous electrolyte, a separator and a cathode and the use of non-aqueous electrolytes possesses serious safety issues due to the flammability and easy ignition of the organic solvents used in these electrolytes (i.e., propylene carbonate, ethylene carbonate, ethylene carbonate) [4–6]. In addition, the growth of Li dendrites in non-aqueous LIBs is unavoidable and can increase the possibility of short-circuiting and limit application in EVs [7–9]. Furthermore, these issues can further be exacerbated in cases of improper use, leading to fires and possible explosions. Moreover, the use of conventional non-aqueous electrolytes also limits the practicality of high-voltage cathode materials to achieve high specific energy batteries [10–12]. Based on these negative attributes, the use of nonflammable solid-state electrolytes to replace non-aqueous electrolytes is considered to be an appealing strategy [13, 14]. Solid-state electrolytes generally include inorganic Li-ion conductors, polymer electrolytes and organic–inorganic hybrid composites [15], and several essential requirements are necessary for their application in LIBs. These include high ionic conductivity ($> 10^{-4}$ S

✉ Jin Yi
jin.yi@shu.edu.cn

Ping He
pinghe@nju.edu.cn

Haoshen Zhou
hszhou@nju.edu.cn

1 Center of Energy Storage Materials & Technology, College of Engineering and Applied Sciences, Jiangsu Key Laboratory of Artificial Functional Materials, National Laboratory of Solid State Microstructures and Collaborative Innovation Center of Advanced Microstructures, Nanjing University, Nanjing 210093, China

2 Institute for Sustainable Energy/College of Sciences, Shanghai University, Shanghai 200444, China

3 Energy Technology Research Institute, National Institute of Advanced Industrial Science and Technology, Umezono 1-1-1, Tsukuba 305-8568, Japan

4 Department of Chemistry, College of Science, Nanjing Agricultural University, Nanjing 210095, Jiangsu, China

cm^{-1}), negligible electronic conductivity, feasible electrochemical stability windows as well as favorable transfer impedance between interfaces [16–18]. Unfortunately, these requirements are difficult to achieve individually or together. For example, although single -ion conductors can avoid concentration polarization effects, their practical application is plagued by low ionic conductivity at room temperature and poor interfacial contact with electrodes. Moreover, the stability of solid-state electrolytes against anode and cathode materials also needs to be taken into consideration. And overall, numerous challenges need to be addressed before commercialization and will require intensive investigation into the fundamentals of solid-state electrolytes. Based on this, extensive research has been carried out recently among industrial and scientific communities to speed up innovation in this field [19–22], and although achievements have been made, the large-scale application of solid-state electrolytes still faces numerous problems ranging from fundamental understanding to industrial manufacturing [23–25]. For example, the mechanism of Li-ion transport remains controversial and has been fiercely debated by researchers for decades, especially around issues associated with Li-ion transport across the interface of anodes, solid-state electrolytes and cathodes, and is a major bottleneck in the practical application of all-solid-state batteries [26]. In addition, aside from the development of advanced characterization techniques, more visual results and direct evidence are required to promote the understanding of fundamentals [27–29]. Based on all of this and to guide future development, this review into solid-state electrolytes will provide the fundamentals of Li-ion transport as well as promising enhancement strategies along with future perspectives and proposed research directions.

2 Overviews of Typical Li-Ion Conductors

2.1 Inorganic Li-Ion Conductors

2.1.1 Oxide-Type Li-Ion Conductors

2.1.1.1 Perovskite Conductors Perovskite (ABO_3)-type Li-ion conductors and structurally related variants have recently attracted extensive attention based on optimal bulk Li^+ conductivities among various solid electrolytes with numerous studies reporting varying ionic conductivities through the replacement of A and B sites with different ions in which ionic conductivities can reach 10^{-3} S cm^{-1} ($x \approx 0.11$) after optimization. The general formula of perovskite-type lithium lanthanum titanate solid-state electrolytes can be expressed as $Li_{3x}La_{(2/3)-x}TiO_3$ (LLTO) with the value of x ranging from 0.07 to 0.13 and the activation energy ranging from 0.3 to 0.4 eV (Fig. 1). Here, the high ionic conductivity of LLTOs is a result of the large concentration of A-site vacancies with researchers reporting that cation deficiencies at A sites as formed by 4 adjacent TiO_6 octahedra can facilitate the migration of Li cations through bottlenecks [30].

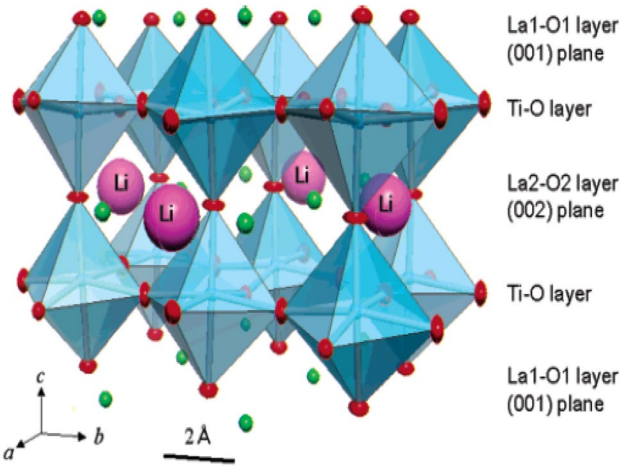

Fig. 1 Crystal structure of $La_{0.62}Li_{0.16}TiO_{3.0}$. Pink, green and blue spheres represent Li, La and Ti atoms, respectively, red ellipsoids represent oxygen ions, and TiO_6 octahedrons are depicted as blue squares. Reprinted with permission from Ref. [31]. Copyright 2005 American Chemical Society

In general, different synthesis methods and heterogeneous lattice vacancies can result in different perovskite-like compounds with diverse crystal structures, including cubic, hexagonal, orthorhombic and tetragonal. And to advance all-solid-state electrolytes, it is essential to probe the ionic conduction mechanism and crystal structure of LLTOs. For example, Bohnke et al. [30] confirmed that the ionic conduction mechanism of LLTOs incorporated the tilting and/or rotation of BO_6 octahedra as promoted by either rising temperatures or increasing vacancies in the structure. Yashima et al. [31] also studied the migration path of the Li-ion conductor $La_{0.62}Li_{0.16}TiO_3$ (Fig. 1) and found that Li cations can migrate from the 2*c* site on the (002) La-deficient layer to the 2*c*-4*f*-2*c* or 2*c*-2*d*-2*c* tie line at 77 K to enhance conductivity.

Overall, perovskite-type conductors are considered to be promising candidates as all-solid-state electrolytes based on their appropriate electrochemical windows and acceptable ionic conductivities; however, the intercalation of Li-ions and limited electrodes greatly restrict practical application.

2.1.1.2 Anti-Perovskite Conductors In 2012, Zhao et al. [32] proposed a new strain of anti-perovskites (LiRAPs) that were "electronically inverted" as compared with standard perovskite-type electrolytes and reported that this novel class of electrolytes can be referred to as anti-perovskites because although they share similar structures with standard perovskite-type electrolytes, the ions of the anti-perovskites in the corresponding lattice sites can undergo electronic

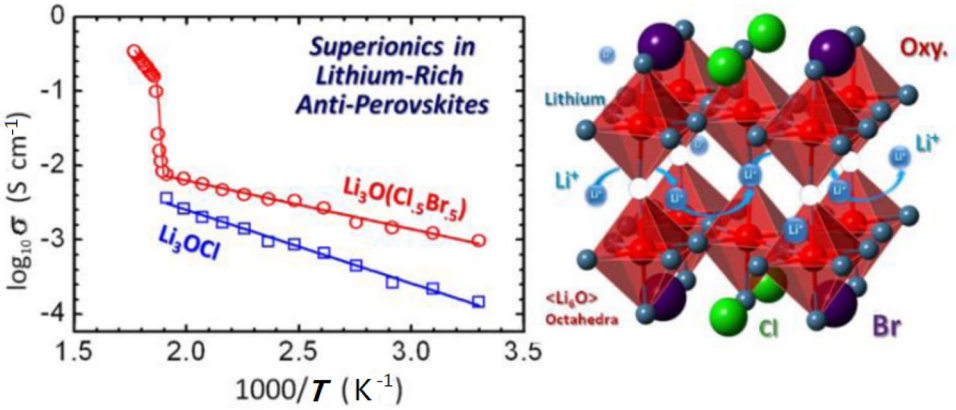

Fig. 2 Left plot denotes the logarithm of the ionic conductivity of Li_3OCl and mixed composite $Li_3OCl_{0.5}Br_{0.5}$ versus $1000/T$ (K^{-1}). The right schematic depicts the structure of $Li_3OCl_{0.5}Br_{0.5}$. Reprinted with permission from Ref. [32]. Copyright 2012 American Chemical Society

inversion. For example, A (monovalent) and B (divalent) can serve as metallic cations in typical ABX_3 perovskite structures with strongly electronegative C anions, whereas A, B and X all possess inverted charges in LiRAP. In addition, B sites located in the octahedral center of LiRAP are occupied by chalcogens^{2-} (O^{2-}, S^{2-}), and any halogens^{-} (F^-, Cl^-, Br^-, I^-) can act as dodecahedral centers (A sites). Here, these researchers reported that the ionic conductivity of LiRAP can reach greater than 10^{-3} S cm^{-1} at ambient temperatures with activation energy of 0.2–0.3 eV and that these LiRAPs possessed good stability even under high temperatures.

Moreover, researchers have reported that chemical substitution can facilely manipulate Li^+ conduction in anti-perovskites. For example, Zhang et al. [33] reported that dodecahedral sites can be supplanted by larger anions (Br^-, I^-) to allow for the replacement of Li with divalent cations (Mg^{2+}, Ca^{2+}, Ba^{2+}) at the Li_6O octahedral center and that the depletion of LiA (samples: $Li_{2.95}OCl_{0.95}$, $Li_{2.90}OCl_{0.90}$, $Li_{2.85}OCl_{0.85}$ and $Li_{2.80}OCl_{0.80}$) can optimize superionic conductivity, in which the conductivity of $Li_3OCl_{0.5}Br_{0.5}$ at room temperature can jump to 6.05×10^{-3} S cm^{-1}. In addition, thermal treatments (i.e., annealing, pressing, heating/cooling) can also affect conductivity in which the ionic conductivity of Li_3OCl, Li_3OBr and $Li_3OCl_{0.5}Br_{0.5}$ (Fig. 2) at ambient temperatures can be significantly enhanced by 2 orders of magnitude after annealed in vacuum for 24*h* [33].

The mechanism of Li^+ transport in LiRAP has also been investigated by Zhang et al. [33], in which phase diagrams and electronic structure calculations proved that anti-perovskites (Li_3OCl, Li_3OBr and their mixed composite $Li_3OCl_{0.5}Br_{0.5}$) were thermodynamically metastable but electrochemically stable. Furthermore, ab initio molecular dynamic simulations were conducted and revealed that increased structural disorders and Li vacancies can lead to enhanced Li^+ diffusion. Despite these results, however, the mechanism of Li-rich anti-perovskites remains a much-debated topic and further studies are needed to address this issue.

As another anti-perovskite, $Li_{3-2x}M_xHalO$ (M stands for divalent cations such as Mg^{2+}, Ca^{2+} or Ba^{2+}, Hal stands for halides such as Cl^-, I^- or a mixture) was first reported by Braga et al. [34] as a novel class of glassy electrolytes based on LiRAP that can exhibit ultra-fast ionic conduction (25 mS cm^{-1} at 25 °C). And based on the merits of these novel glassy electrolytes (lightness, nonflammability, non-polluting, thermal and electrochemical stability, etc.), they are expected to be promising in future applications in which higher valence dopants can result in higher conductivities.

2.1.1.3 NASICON Conductors As another oxygen type of Li conductors, NASICON-type conductors ($Na_{1+x}Zr_2P_{3-x}Si_xO_{12}$) are promising fast ion conductors with high conductivity that are derived from $NaZr_2(PO_4)_3$ after the replacement of P with Si due to the poor ionic conductivity of P. Here, researchers have reported that the enhanced conductivity of $Na_{1+x}Zr_2P_{3-x}Si_xO_{12}$ can be attributed to 3 reasons, including the increased mobility of Na^+ ions in the structure, the higher density of the sintered pellets and the more favorable environment for Na^+ ion migration through the 3D structure with enlarged tunnel sizes [35]. Of these NASICON-type conductors, iso-structural $LiM_2(PO_4)_3$ (M = Zr, Ti, Hf, Ge or Sn) was first reported in 1977 in which the skeletons consisting of MO_6 octahedra and PO_4 tetrahedra sharing oxygen atoms (Fig. 3) [36]. These $LiM_2(PO_4)_3$ series can further be divided into $LiM_2(PO_4)_3$ (M = Ti, Ge) with rhombohedral symmetry and $LiM_2(PO_4)_3$ (M = Zr, Hf, or Sn) with a triclinic phase and lower symmetry. Here, alkaline ions in the rhombohedral phase are likely to occupy two crystallographic sites in which M1 sites are surrounded by 6 oxygens and M2 sites are positioned between 2 adjacent M1 positions with tenfold oxygen coordination. As for the triclinic phase, Li cations are driven by structural distortions in a fourfold coordination at the intermediate M12 sites. In addition, researchers have reported that the conductive performance of $LiTi_2(PO_4)_3$ outshines other $LiM_2(PO_4)_3$ (M = Zr, Ge or Hf) materials because of its optimal lattice size for conducting Li^+ ions. Moreover,

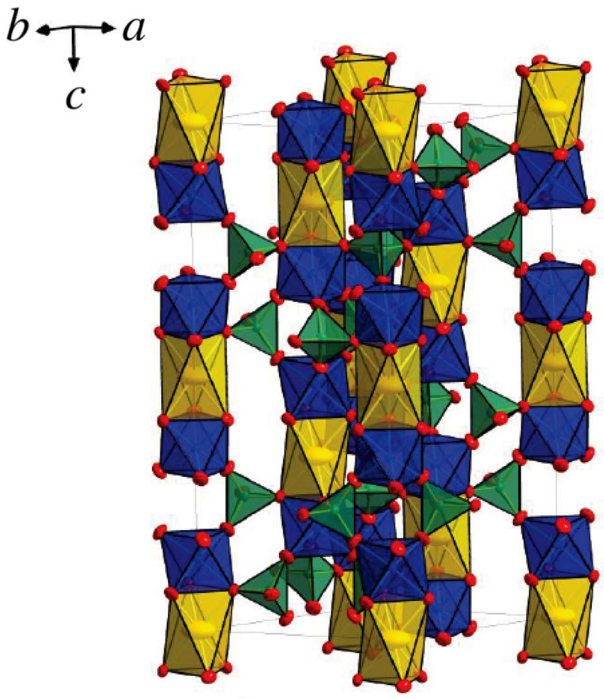

Fig. 3 Unit cell of $LiTi_2(PO_4)_3$. Li^+, Ti^{4+} and P^{5+} occupy yellow octahedra, blue octahedra and green tetrahedra, respectively. Reprinted with permission from Ref. [36]. Copyright 2017 American Chemical Society

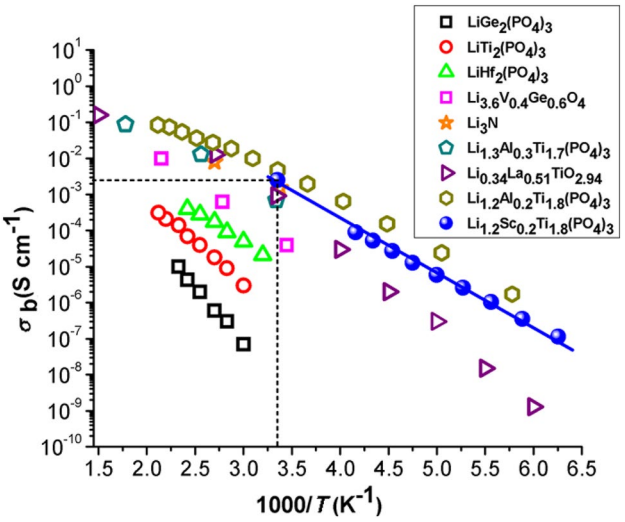

Fig. 4 Ionic conductivity of NASICON-type Li-ion solid electrolytes. Reprinted with permission from Ref. [37]. Copyright 2017 American Chemical Society

researchers have also reported that trivalent cations such as Al^{3+}, Sc^{3+}, Ga^{3+}, Fe^{3+}, In^{3+} and Cr^{3+} replacing partial Ti^{4+} cations in $Li_{1+x}R_xTi_{2-x}(PO_4)_3$ can enhance conductivity in which $Li_{1.3}Al_{0.3}Ti_{1.7}(PO_4)_3$ (LATP) can gain an enhanced ionic conductivity of 7×10^{-4} S cm^{-1}. Furthermore, the ionic radius of M^{4+} cations can influence the lattice constants of $LiM_2(PO_4)_3$ (M = Ge, Hf, or Zr) as well to further contribute to the tunnel size for Li^+ diffusion (Fig. 4) [37]. Augmenting densification, increasing the mobile ion content in the structure and reducing activation energy derived from the incorporation of trivalent ions can also enhance ionic conductivity in NASICON-type conductors [35]. In another study, Arbi et al. [37] also investigated the influence of cation miscibility in the optimization of the transport properties of $Li_{1+x}Ti_{2-x}Sc_x(PO_4)_3$ ($0\le x\le0.5$) series and reported that in Sc-poor samples, NASICON phases with rhombohedral symmetry were characterized by using XRD patterns whereas in Sc-rich structures, the existence of secondary TiO_2, $LiScO_2$ and $LiScP_2O_7$ phases was confirmed, which were found to suppress the incorporation of Li in the NASICON phase. Furthermore, Aono et al. [35] proposed another strategy to enhance conductivity by introducing secondary Li compounds including Li_2O, Li_3PO_4 and Li_3BO_3 to serve as fluxes to promote crystallization and form conductive components at the grain boundary in which the addition of 20% Li_2O into $LiTi_2(PO_4)_3$ leads to a constant conductivity of 5×10^{-4} S cm^{-1}.

2.1.1.4 Garnet-Type Conductors In 2003, a novel family of Li-ion electrolytes possessing a garnet-like structure and a nominal composition of $Li_5La_3M_2O_{12}$ (M = Nb, Ta) was proposed by Thangadurai et al. [38] that has since attracted wide interest due to unique crystal structures, high conductivities and wide electrochemical windows, in which compared with LiPON, Li_9AlSiO_8 and Li-β-alumina, the ionic conductivity of these garnet-type conductors was higher and the bulk conductivity of both niobium and tantalum compounds could reach a similar order of magnitude (~ 10^{-6} S cm^{-1} at 25 °C) with activation energy of 0.43 eV and 0.56 eV, respectively. In addition, the Ta members ($Li_5La_3Ta_2O_{12}$) were also chemically stable in molten Li and moisture.

Of these garnet-type conductors, orthosilicate garnets possess the formula $A_3^{II}B_2^{III}(SiO_4)_3$ in which A and B stand for 8- and 6-coordinated cation sites. And in this structure, separated SiO_4 tetrahedra are bonded to each other through ionic bonds between interstitial B cations and by replacing silicon with other elements, various complex oxides have been revealed to crystallize in the garnet-like conductors with a general formula of $A_3B_5O_{12}$ (A = Ca, Mg, Y or Ln = La, or rare-earth elements; B = Al, Fe, Ga, Ge, Mn, Ni, V), resulting in a 3D structure made up of BO_4 tetrahedra and BO_6 octahedra sharing corners with each other. For example, in the crystal structure of $Li_5La_3M_2O_{12}$ (M=Nb, Ta) (Fig. 5), 8- and 6- coordination sites are occupied by La and Ta ions with Li-ions on both the octahedral and tetrahedral sites as confirmed by neutron diffraction investigations

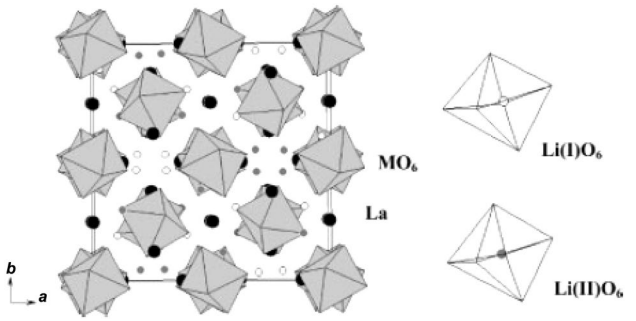

Fig. 5 Crystal structure of $Li_5La_3M_2O_{12}$(M = Nb, Ta). Reprinted with permission from Ref. [42]. Copyright 2005 John Wiley and Sons

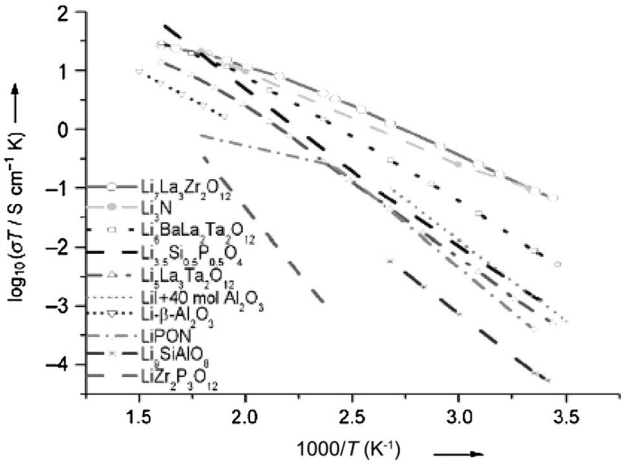

Fig. 7 Comparison of the total conductivity of $Li_7La_3Zr_2O_{12}$ and other Li-ion conductors. Reprinted with permission from Ref. [44]. Copyright 2007 John Wiley and Sons

[38] in which Li(I)O_6 was much more distorted than Li(II)O_6. In addition, researchers have also reported that 6 LiO_6 octahedra and 2 vacant sites of Li-ions surrounding MO_6 octahedra can result in high Li-ion conduction [39]. Thangadurai et al. [40] also enhanced the ionic conductivity of garnet-like $Li_5La_3Nb_2O_{12}$ through the partial substitution of K^+ for La^{3+} and In^{3+} for Nb^{5+}. These researchers also reported that high sintering temperatures can decrease grain boundary resistances and create large grain size particles to fashion microstructures and enhance conductivity. Moreover, Thangadurai et al. [41, 42] in subsequent studies generated original garnet-like conductors through the replacement of La with alkaline earth elements and reported that ionic conductivity reduced as the ionic radius of alkaline earth ions decreased in which among various conductors synthesized, Ba compound $Li_6BaLa_2Ta_2O_{12}$ showed optimal ionic conduction performances (4×10^{-5} S cm^{-1} at room temperature with activation energy of 0.40 eV). These researchers also reported that the ionic conductivity of parent compound $Li_5La_3Nb_2O_{12}$ can be enhanced by Y- and Li-codoping to create a novel Li-rich $Li_{5+2x}La_3Nb_{2-x}Y_xO_{12}$ structure in which trivalent ions such as Y^{3+} surpassed other dopants such as M^{2+} (alkaline earth ions), In^{3+} and Zr^{4+} [43].

Cubic $Li_7La_3Zr_2O_{12}$ (LLZO) is another garnet-like structure (Fig. 6) that was first demonstrated by Murugan et al. [44] and is a promising all-solid-state ion conductor that possesses a higher total conductivity (3×10^{-4} S cm^{-1}) than that of any previously reported Li garnet-like materials (Fig. 7). Here, researchers report that in cubic LLZO, Li-ions are distributed over the octahedral 48*g*, tetrahedral 24*d* Li(1) and 96*h* Li(2) sites [45]. Another tetragonal-type LLZO polymorph with low-temperature tetragonal symmetry was also reported; however, the well-ordered arrangement of Li-ions at the octahedral 16*f* and 32*g* sites and tetrahedral 8*a* sites resulted in a much lower conductivity value of 10^{-6} S cm^{-1} [46, 47]. As a result, many studies have been devoted to the stabilization of cubic structures in garnet-type conductors

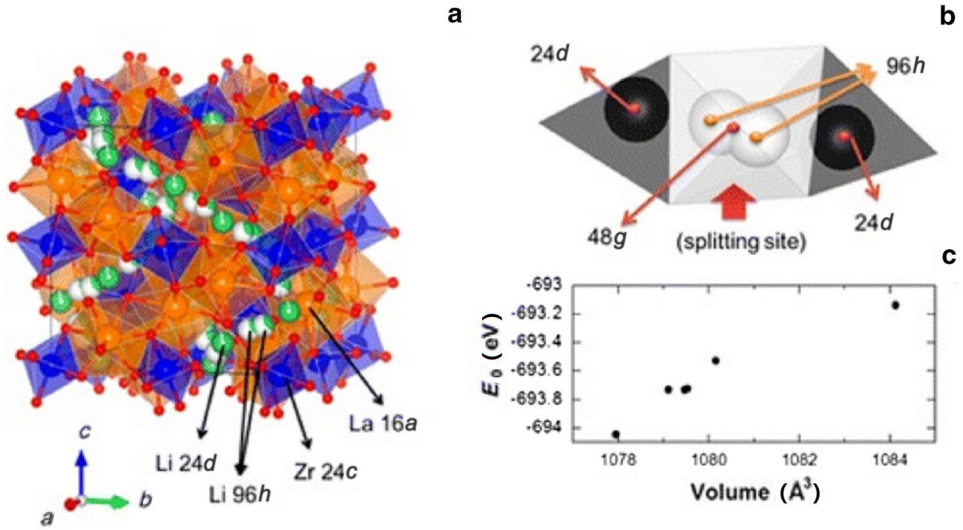

Fig. 6 Crystal structure of cubic LLZO. Li-ions distributed over the octahedral 48*g*, tetrahedral 24*d* Li(1) and 96*h* Li(2) sites. Reprinted with permission from Ref. [45]. Copyright 2013 American Chemical Society

either through the increase in Li vacancy concentrations or the reduction in the Li content. For example, Rangasamy et al. [48] demonstrated that the addition of Al as a substitute for Li can generate more Li vacancies and investigated the optimal ratio of Al to Li to form desirable LLZOs.

The Li-ion diffusion mechanism of garnet-type conductors is also controversial; however, better understandings of Li^+ transport mechanisms require advanced characterization techniques to determine the exact location of Li-ions. For example, Thangadurai et al. [49] utilized the bond valence sum method to explore the characteristic structure of $Li_5La_3M_2O_{12}$ and confirmed possible ion transport pathways through a minimization procedure of bond valence mismatch in which the obtained results revealed that Li-ions exclusively occupied octahedral sites. However, Cussen et al. [50] later disputed this finding and proposed that Li-ions in the framework of $Li_5La_3M_2O_{12}$ (M=Ta, Nb) were located in both octahedral and tetrahedral sites in which Li^+ in the octahedra sites was a mobile species whereas Li^+ in the tetrahedral sites was considered to be trapped and immobile. This conclusion was also reached by Wüllen et al. [51] employing advanced NMR strategies. Furthermore, researchers have also reported the significance of final annealing temperatures because the mobility of Li-ions is sensitive to Li-ions migration. For example, annealing with high temperatures can facilitate more Li-ions in octahedral sites to improve ionic conductivity. As for the migration mechanism of LLZOs, this is typically determined by the imposed restrictions of occupied site-to-site interatomic isolation allowing only 48*g*/96*h*-24*d*-48*g*/96*h* and the temporal stay of Li^+ at the 24*d* site which can promote ion mobility and reconfigure surrounding Li neighbors [45]. In addition, simulation methods are useful tools to gain deeper understandings of migration mechanisms in which Xu et al. [52] use the nudged elastic band (NEB) method to find the minimum energy path for Li diffusion in $Li_{3+x}La_3M_2O_{12}$($x=0$, 2, 4).

2.1.2 Sulfide-Type Li-ion Conductors

2.1.2.1 Thio-LISICONs The thio-LiCICONs family has been proposed as a sulfide-type Li-ion conductor due to its enhanced electrochemical performance as compared with LISICON family conductors and can be described through the nominal composition of $Li_{4-x}M_{1-y}M'_yS_4$ (M = Si, Ge, and M' = P, Al, Zn, Ga) [53, 54]. And among these conductors, the ionic conduction of $Li_{4-x}Ge_{1-x}P_xS_4$ (2.2×10^{-3} S cm^{-1} at 25 °C) showed superior performances than any other members. Researchers have also reported that ionic conduction performances are mainly dependent on the radius and polarizability of constituted ions in which the replacement of O by S can diminish interactions between Li^+ in the sublattice and increase the concentration of mobile Li^+, which explains the higher conductivity of S-doped LISICONs as compared with their oxide analogues.

Kamaya et al. [55] also developed a novel crystalline sulfide Li-ion electrolyte ($Li_{10}GeP_2S_{12}$) with outstanding electrochemical properties (exceedingly high conductivity of 1.2×10^{-2} S cm^{-1} and a wide potential window) and other advantages and reported that this material can be applied in LIBs with $LiCoO_2$ and Li-In alloy as the cathode and the anode, respectively, to achieve desirable performances. Here, the researchers determined the crystal skeleton of $Li_{10}GeP_2S_{12}$ using XRD and synchrotron radiation X-ray data associated with the ab initio method to reveal a 3D framework with LiS_6 octahedra and ($Ge_{0.5}P_{0.5}$) S_4 tetrahedra forming 1D chains connected by a common edge, which are connected at the corners with PS_4 tetrahedra. In addition, neutron Rietveld analysis was used to further confirm Li occupation and the Li content. Du et al. [56] also reported that tetrahedrally coordinated Li1 (16*h*) and Li3 (8*f*) sites were responsible for ionic conduction and formed a 1D tetrahedral chain along the *c* direction whereas the octahedrally coordinated Li2 sites were not available for Li^+ diffusion, suggesting that Li^+ diffusion paths along the *c*-axis were better for Li^+ diffusion than that in the *ab* plane (reflecting only weak anisotropy of Li^+ diffusion) with the thermodynamic stability being studied by using ab initio methods. Furthermore, the strong Coulombic connection between mobile ions can prompt Li-ion transport in a string-like manner in LGPS with low activation energy barriers and extremely high ionic conductivities [57].

2.1.2.2 LGPS Family Since being first proposed in 2011, $Li_{10}GeP_2S_{12}$ (LGPS) has attracted wide interest due to an incredible ionic conductivity that is comparable to organic liquid electrolytes (Fig. 8) [55]. However, the unstable interface of LGPS needs to be addressed [58] as well as the low abundance and high cost of Ge in the electrolyte. Based on this, the exploration of new LGPS-type materials is necessary to advance the application of LGPS conductors in which the LGPS family can be divided into Ge-free and Ge-doped electrolytes ($Li_{10}GeP_2S_{12}$ and Li_7GePS_8) [59].

To address the high cost of Ge, researchers have attempted to substitute Ge^{4+} with homologous Si^{4+} or Sn^{4+}, resulting in materials such as $Li_{10}SnP_2S_{12}$ [60], $Li_{10+\delta}(Sn_ySi_{1-y})_{1+\delta}P_{2-\delta}S_{12}$ [61], $Li_{11}Si_2PS_{12}$ [62], $Li_{9.54}Si_{1.74}P_{1.44}S_{11.7}Cl_{0.3}$ [63]. And overall, researchers report that these Si- and Sn-doped materials exhibited lower conductivities than parent LGPS in which Si-doping, to some extent, can narrow tunnel sizes for Li migration and lower conductivity. As for the reduction in conductivity in Sn analogues, Zeier et al. [64] in their study clearly found that Sn^{4+} substitution can render the bottleneck of Li^+ diffusion along

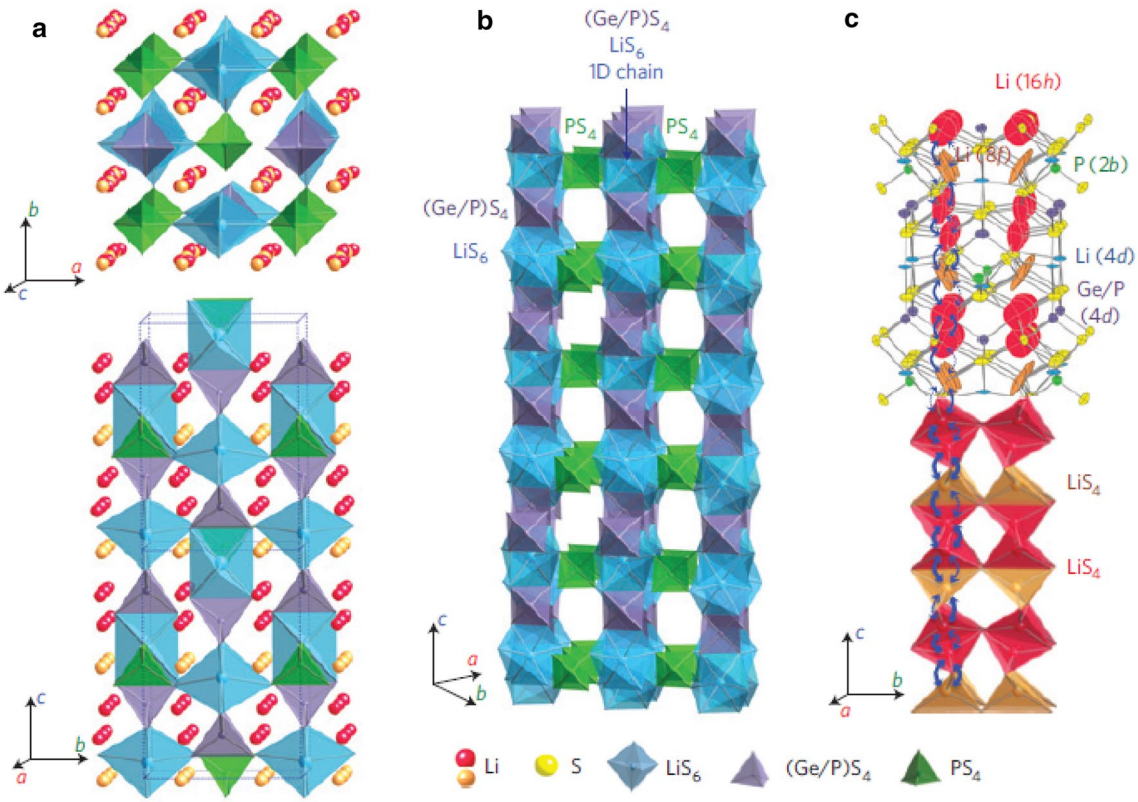

Fig. 8 **a** Framework structure and Li-ion environment of $Li_{10}GeP_2S_{12}$. **b** Framework of $Li_{10}GeP_2S_{12}$. **c** Conduction pathway of Li-ions in $Li_{10}GeP_2S_{12}$. Reprinted with permission from Ref. [55]. Copyright 2011 Nature Publishing Group

the *z*-direction, which induces tougher activation barriers. And of these substituted LGPSs, Kato et al. [63] reported that $Li_{9.54}Si_{1.74}P_{1.44}S_{11.7}Cl_{0.3}$ possessed an exceedingly high conductivity of up to 25 mS cm^{-1}, which was the highest ever reported for Li conductors (specific data demonstrated in Fig. 9a) and double that of the archetype LGPS [63]. Here, the researchers used the anisotropic thermal displacement of Li (Fig. 9b) and nuclear density distribution (Fig. 9c) to verify 3D Li migration channels with 1D channels along the *c*-axis and 2D channels in the *ab* plane and suggested that this 3D conduction pathway in the LGPS-type conductor can contribute to optimal conductivities. In addition, these researchers also reported good chemical stability of the LGPS-type conductor, especially at 100 °C, and attributed this to the lack of elemental diffusion and small interfacial resistance. Moreover, $Li_{9.6}P_3S_{12}$ also possesses a similar LGPS structure and has been reported to also possess excellent electrochemical stability and longer lifespans under extreme cell operation conditions. Recently, Sun et al. [61] also successfully obtained a Sn-Si derivative of LGPS-type conductors [$Li_{10+\delta}(Sn_ySi_{1-y})_{1+\delta}P_{2-\delta}S_{12}$] in the form of a Li_3PS_4-Li_4SnS_4-Li_4SiS_4 quasi-ternary system in which the researchers reported that by adjusting the ratio of Sn/Si and M^{4+} (Sn^{4+} and Si^{4+})/P^{5+} in the [M1/P1] (4*d*) site, the dual doping of the original LGPS with Sn and Si can improve ionic conduction, resulting in a $Li_{10.35}(Sn_{0.27}Si_{1.08})P_{1.65}S_{12}$ achieving an ionic conductivity of 1.1×10^{-2} S cm^{-1} that is extremely close to that of the archetype LGPS (1.2×10^{-2} S cm^{-1}).

2.1.2.3 Argyrodites Argyrodites are characterized by high ionic conductivities and good cation mobility, and fast Li-ion conducting argyrodites such as Li_6PS_5X (X = Cl, Br, I) are representative members of this family. Here, the addition of halides into argyrodites can lead to conductivities in the range of 10^{-2}–10^{-3} S cm^{-1} in which Deiseroth et al. [65] reported that Li_6PS_5X can be formed by mixing Li_2S, P_2S_5 and LiX under 550 °C and that Li_6PS_5Cl and Li_6PS_5Br showed better conductivity than Li_6PS_5I. As for the crystal structure of Li_6PS_5X (Fig. 10a), the framework of the lattice is based on a cubic Laves topology and PS_4^{3-} anions are located in the middle of 4*b* sites whereas the remaining sulfur atoms take up 4*a* and 4*c* sites [66]. Here, despite the replacement of sulfur by halogens, the sulfur of PS_4^{3-} is not substituted and halogens take up 4*a* or 4*c* sites to display a face-centered structure in which the remaining tetrahedral interstices (24*g* and 48*h* Wyckoff sites) are occupied by Li-ions. In addition, position 24*g*

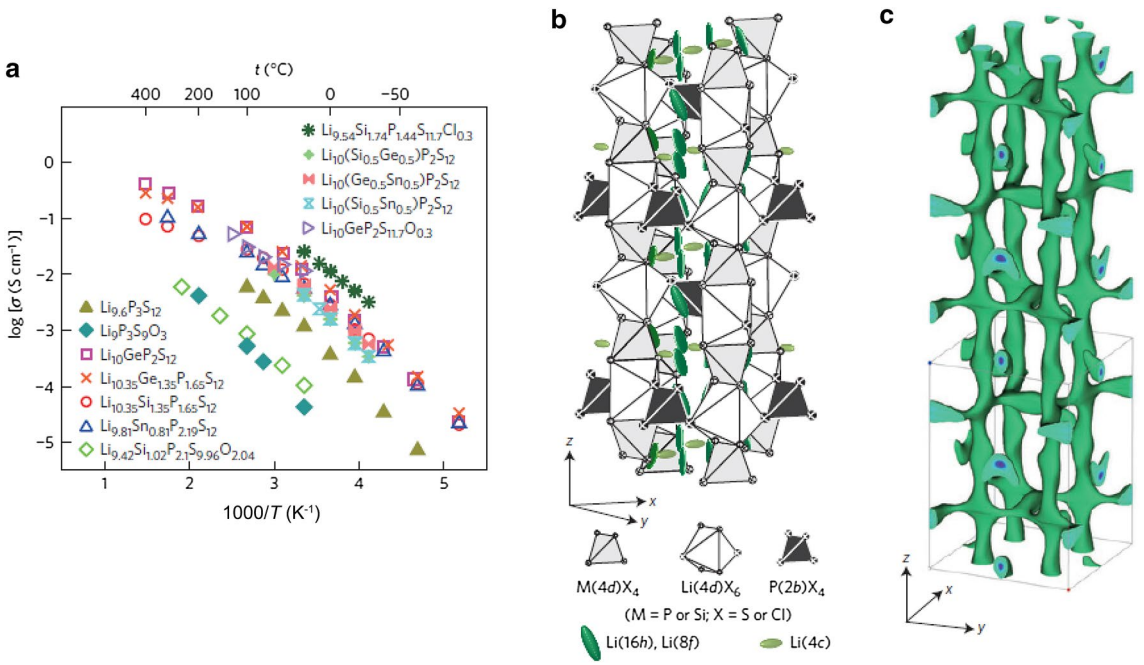

Fig. 9 Ionic conductivity and framework of $Li_{9.54}Si_{1.74}P_{1.44}S_{11.7}Cl_{0.3}$. **a** Arrhenius conductivity plots for the LGPS family, $Li_{9.6}P_3S_{12}$ and $Li_{9.54}Si_{1.74}P_{1.44}S_{11.7}Cl_{0.3}$. **b** Framework structure of $Li_{9.54}Si_{1.74}P_{1.44}S_{11.7}Cl_{0.3}$. **c** Nuclear distributions of Li atoms in $Li_{9.54}Si_{1.74}P_{1.44}S_{11.7}Cl_{0.3}$ at ambient temperature. Reprinted with permission from Ref. [63]. Copyright 2016 Nature Publishing Group

can serve as the transition state for jumps between 2 48*h* sites and 12 48*h* sites can constitute a cage structure by surrounding each 4*c* site (Fig. 10b).

As for Li diffusion caused by these partially occupied positions, this can be attributed to 3 different jump processes, including next-neighbor jumps (48*h*–24*g*–48*h*), intra-cage jumps (48*h*–48*h* jumps within the cage) and inter-cage jumps (48*h*–48*h* jumps between cages) [66]. And among these processes, inter-cage jumps are considered to play a dominate role in macroscopic long-range ion transport whereas intra-cage jumps with low jump rates can constrain diffusion (Fig. 9c, d) [23, 67]. In addition, the replacement of sulfur with halogen can generate vacancies, which is associated with disorder on the S^{2-}/X^{-} sublattice and can enhance local Li-ion diffusion. For example, Deiseroth et al. [65] reported that Cl^{-1} and Br^{-1} can take up 4*a* and 4*c* sites in Li_6PS_5X to allow for the significant disordering of halogen ions, resulting in high conductivities for Li_6PS_5Cl and Li_6PS_5Br. Alternatively, I^{-1} can barely takes up 4*a* sites and I-containing argyrodites lacking the disorder to display higher activation barriers for conduction. In addition, Kraf et al. [66] reported the effect of lattice dynamics on ionic motion and concluded that the migration barrier of moving cations decreases with softer lattices.

2.1.2.4 Other New Thiophosphates Aside from the above thiophosphates, several novel sulfide-based Li-ion conductors with different features have also been recently reported in which Li_4PS_4I as a superionic conductor is one representative example. Here, Sicolo et al. [68] synthesized Li_4PS_4I using a solvent-based method in which Li_4PS_4I presented a new structure that was composed of insular PS_4^{3-} tetrahedra aligned by layers vertical to the *c*-axis and Li-ions were dispersed over 5 partially occupied sites and diffused in a 3D migration pathway. And according to topo-structural analyses, the Li-ion conductivity of the Li_4PS_4I was $\sim 1.2\times10^{-4}$ S cm^{-1} and based on recent calculations, a higher conductivity $> 10^{-2}$ S cm^{-1} is attainable [68].

Minafra et al. [69] also synthesized superionic Li-argyrodite $Li_{6+x}P_{1-x}Si_xS_5Br$ through aliovalent doping into argyrodites and through X-ray, neutron diffraction and electrochemical impedance spectroscopy, reported that the $Li_{6+x}P_{1-x}Si_xS_5Br$ exhibited both structural changes and a threefold enhancement in ionic conductivity as compared with non-doped argyrodites. Here, the researchers suggested that the expansion of unit cells can be explained by the substitution of P^{5+} with larger Si^{4+} and the inclusion of additional Li^+, with the increasing Li content leading to increasing occupancy of Li^+ on the transition states and therefore improved transport properties.

More recently, theoretical studies have also revealed that $Li_{1+2x}Zn_{1-x}PS_4$ (LZPS) as characterized by a body-centered-cubic structure can provide high Li-ion conductivity in which Richards et al. [70] employed AIMD and DFT to study the LZPS and reported that $Li_{1+2x}Zn_{1-x}PS_4$ with higher

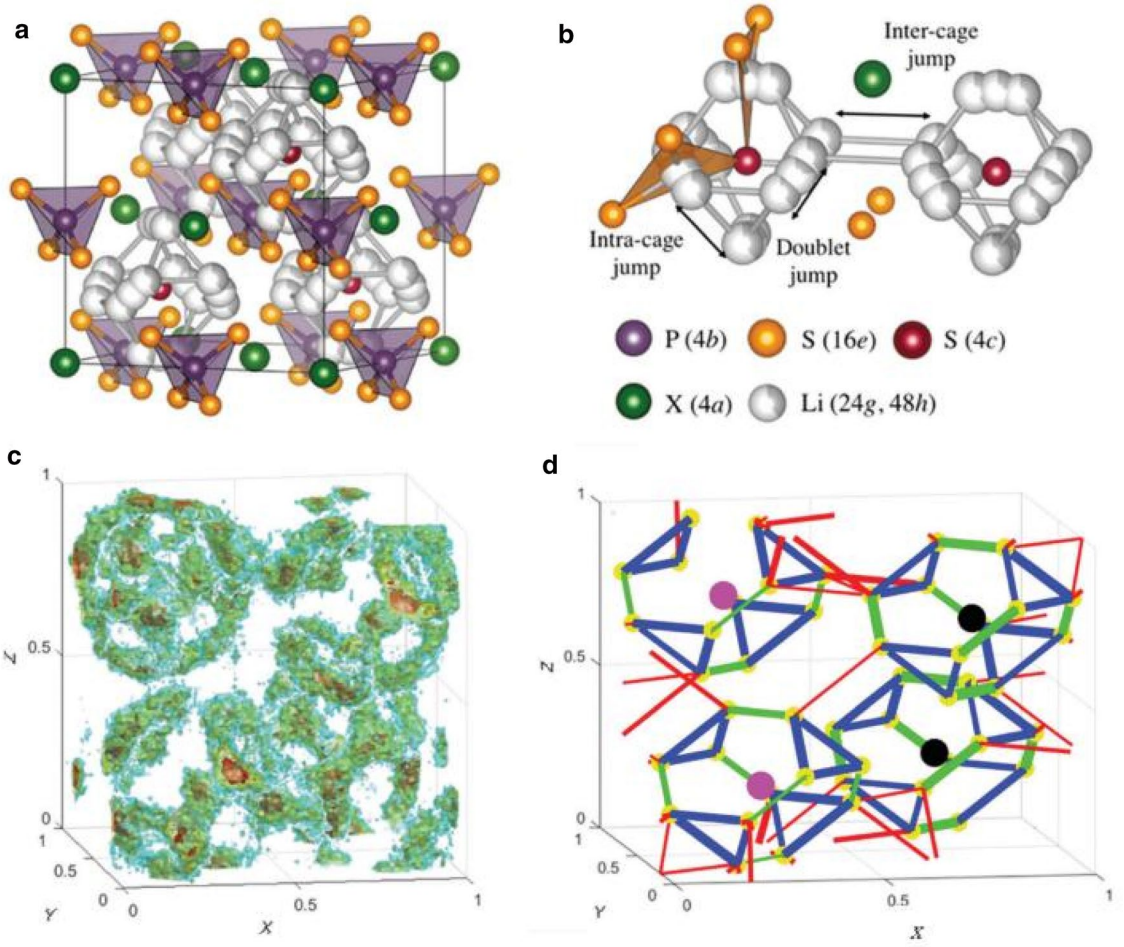

Fig. 10 **a** Crystal structure of Li_6PS_5X. **b** Li positions and possible jump routes. **c** MD simulation of Li-ion density in Li_6PS_5Cl. **d** MD results of jump statistics of Li_6PS_5Cl. Reprinted with permission from Ref. [23]. Copyright 2018 Royal Society of Chemistry

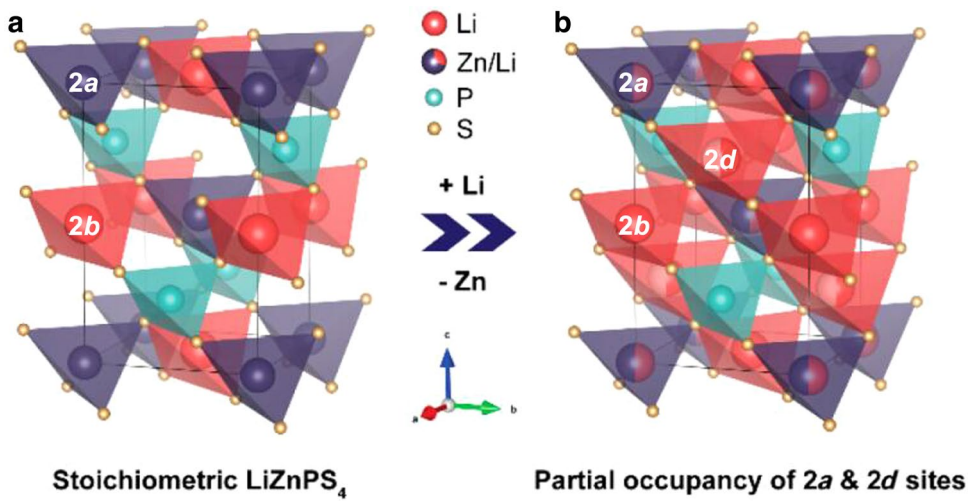

Fig. 11 Crystal structures of **a** stoichiometric and **b** nonstoichiometric $LiZnPS_4$. Reprinted with permission from Ref. [71]. Copyright 2018 American Chemical Society

x can exhibit lower Li migration barriers. Here, the structure of the parent phase stoichiometric $LiZnPS_4$ (Fig. 11a) is composed of $PS_4^{3-}$and ZnS_4^{6-} tetrahedra in which Li takes over 2*b* sites and Zn distributes over 2*a* sites. As for the crystal structure of $Li_{1+2x}Zn_{1-x}PS_4$ ($x>0$) (Fig. 11b), these researchers reported that excess Li-ions can share 2*a* sites

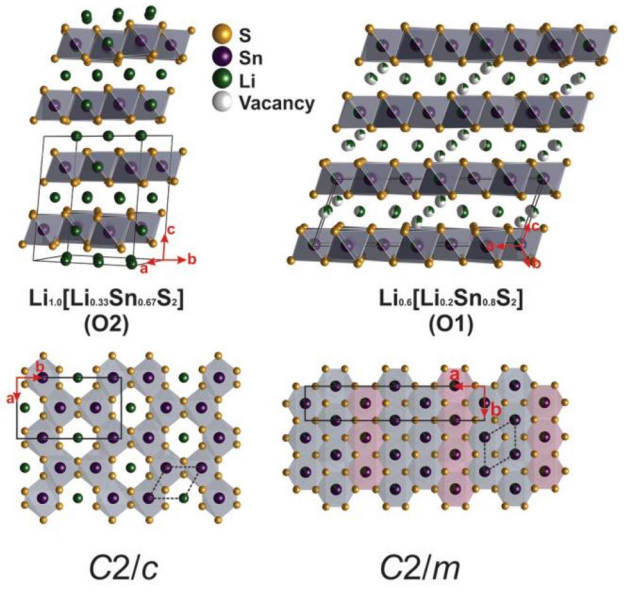

Fig. 12 Left: Crystal structure of $Li[Li_{0.33}Sn_{0.67}S_2]$ with a full Sn/Li order. Right: crystal structure of $Li_{0.6}[Li_{0.2}Sn_{0.8}S_2]$ with partially substituted Sn positions and an O1 type stacking. Reprinted with permission from Ref. [75]. Copyright 2016 Royal Society of Chemistry

with Zn and occupy 2*d* sites that are charge compensated due to the replacement of Zn^{2+} in the 2*a* sites by Li^+. Kaup et al. [71] also synthesized a well-crystallized LZPS with a high *x* value of 0.35 and reported that the resulting $Li_{1.7}Zn_{0.65}PS_4$ can exhibit high conductivities of $> 10^{-4}$ S cm^{-1}, which the researchers attributed to the Li occupation over 2*d* interstitial sites and decreased Li-ion migration barriers [72]. Despite these performances, however, the conductivities of these experimental $Li_{1+2x}Zn_{1-x}PS_4$ samples were all lower than those obtained through theoretical calculations, which may be due to the amorphous content and highly metastable defect composition. In addition, studies have revealed that $Li_{2.5}Zn_{0.25}PS_4$ with a glassy matrix can provide conductivities up to 8×10^{-4} S cm^{-1}.

2.1.2.5 Layered Sulfides Recently, a series of fast Li-ion conductors based on $Li_{3x}[Li_xSn_{1-x}S_2]$ has been identified in which $Li[Li_{0.33}Sn_{0.67}S_2]$ (Li: Sn = 1: 2) and $Li_{0.6}[Li_{0.2}Sn_{0.8}S_2]$ (Li: Sn = 1: 4) are two outstanding examples that can exhibit different structures and ion conductivities. Here, both layered sulfides can be synthesized by using several approaches such as a facile wet chemistry approach for both [73], a high-temperature solid-state approach for Li_2SnS_3 ($x = 0.33$) [74] and other methods for $Li_2Sn_2S_5$ ($x = 0.2$) [75]. And in the case of the Li-rich prototype Li_2SnS_3 (in *C*2/*c*), Brant et al. [74] reported the crystallization of Li_2SnS_3 in a layered A_2BO_3 structure with a NaCl-like network (Fig. 12), in which the framework was built up by Li/Sn-ordered sulfide layers with Sn ions being arranged in a honeycomb fashion

Table 1 Ionic conductivities of representative crystalline inorganic solid Li-ion conductors at room temperature

Electrolyte	Ionic conductivity (S cm^{-1})	References
$Li_{3x}La_{(2/3)-x}TiO_3$	10^{-3}	[30, 31]
LiRAP	10^{-3}	[32]
$LiM_2(PO_4)_3$	10^{-3}–10^{-4}	[35–37]
$Li_5La_3M_2O_{12}$	10^{-4}–10^{-6}	[38–50, 52]
$Li_{4-x}M_{1-y}M'_yS_4$	10^{-2}–10^{-3}	[53–57]
LGPS	1.1×10^{-2}–10^{-4}	[58, 59, 61–64]
Li_6PS_5X	10^{-2}–10^{-3}	[23, 65–67]
$Li_{1+2x}Zn_{1-x}PS_4$	~10^{-4}	[70–72]
$Li_{3x}[Li_xSn_{1-x}S_2]$	~10^{-5}	[73–75]

and Li-ions being sandwiched between the layers, showed an ionic conductivity of 1.5×10^{-5} S cm^{-1} at room temperature and 1.6×10^{-3} S cm^{-1} at 100 °C. As for the Li-depleted version, Holzmann et al. [75] reported that the structure of $Li_2Sn_2S_5$ (in *C*2/*m*) was similar to the parent compound Li_2SnS_3 whereas the Li content decreased to 60% in the interlayer gallery (Fig. 12). Here, these researchers reported that the Li depopulation resulted in an increase in the interlayer distance due to charge compensation by additional Sn in the honeycomb layers as well as the enhancement of Li mobility in the interlayer gallery, which contributed the most to high ionic conductivities. And based on impedance spectroscopy, these researchers reported that the activation energy of $Li_2Sn_2S_5$ was 0.17 eV, which was lower than that of Li_2SnS_3 (0.59 eV) and attributed this to the different Li diffusion pathways in which for $Li_2Sn_2S_5$, there was an addition diffusion pathway of hops between tetrahedral (T) and face-sharing octahedral (O) Li sites as compared with the pure O–O trajectories in $Li_2Sn_2S_5$. And as a result, $Li_2Sn_2S_5$ is the best Li solid electrolyte currently based on a bulk conductivity of $\sigma_{NMR} = 9.3 \times 10^{-3}$ S cm^{-1} by using data taken from field gradient (PFG) NMR which is consistent with a conductivity of 1.5×10^{-2} S cm^{-1} as measured by impedance spectroscopy. Furthermore, in the case of single-crystalline $Li_2Sn_2S_5$ samples, even higher conductivities are possible along the *ab* plane based on structural anisotropy (Table 1).

2.2 Polymer Electrolyte-Based Li-ion Conductors

All-solid-state electrolytes consist of inorganic solid electrolytes (ISEs), solid polymer electrolytes (SPEs) and organic–inorganic hybrid electrolytes [25]. And although this review primarily presents typical organic Li-ion conductors (oxide-based or sulfide-based materials), it is still necessary to provide a brief overview of solid polymer electrolytes (SPEs) and organic–inorganic hybrid materials due to their wide application in Li batteries.

2.2.1 Polyether-Based SPEs

In 1973, Wright et al. [76] first reported the successful synthesis of crystalline alkali metal salt complexes of poly(ethylene oxide) (PEO) with ionic conduction. And since 1978, SPEs have been considered as candidates for application in electrochemical devices due to a combination of solid-state electrochemical properties and facile processability inherent to plastics [77]. SPEs are solid solutions of alkali metal salts in polymer matrixes without the presence of organic liquid solvents. These electrolytes possess many advantages over liquid electrolytes, including the lack of leakage, low flammability, absolute safety, great flexibility and facile processability [78, 79]. And of the many SPEs, PEO is a semi-crystalline polymer that can enable interconnection between Li^+ ions and oxygen atoms in the PEO matrix [80]. Here, it is widely acknowledged that the mobile and disordered Li transport of PEO SPEs can be ascribed to the continuous segmental motion of the PEO chain to transfer Li^+ ions to the surrounding chains and create new sites [80, 81]. However, the motion of PEO chains can be negatively affected by decreased temperatures and aggravated crystallinity, thus restricting practical application [25]. To address this, researchers have reported that the potential solution to promote the segmental movement of SPEs is to reduce the presence of crystalline domains because amorphous phases are mainly accountable for high ionic conductivity in polymer materials rather than crystalline domains [79].

In addition, researchers have also reported that the suitable glass transition temperature (T_g) of materials is a major factor for high ionic conductivity because the movement of amorphous polymer chain segments is continuous only above T_g, which is crucial to facilitate the transport of ions [82]. And although elevated temperatures can to some extent expand the amorphous region and reinforce interfacial stability with electrodes [83, 84], high temperatures over 80 °C can result in growth of Li dendrites and limited electrochemical windows [85]. Therefore, ideal polymer electrolytes should possess a low T_g to maintain conductivity even at room temperature and preserve good ionic conductivity [86].

Furthermore, efforts have been made to inhibit crystallization, which has major implications in ionic conductivity in which the most common method is the addition of liquid plasticizers into PEO-LiX matrixes. However, this method can also reduce the intrinsic nature of polymer electrolytes due to solid-state deconfiguration and less compatibility with electrodes. Researchers have also suggested the addition of ceramic powder into PEO-type polymer electrolytes to enhance mechanical and interfacial properties and, most importantly, low-temperature conductivity [87–90]. Moreover, researchers have also reported that smaller nanosized ceramic powders (TiO_2, SiO_2, Al_2O_3 [91] and MgO [92]) can better retard crystallization. In addition, blend-based polymers [93–96] and copolymerization with other polymers [85, 97, 98] have also been proposed as effective means to develop amorphous polymer matrixes to reduce the possibility of increasing crystallization. Other polyethers such as PPO [99, 100] and nitrile-based polymer electrolytes such as PAN [101–103] have also have been reported. However, due to the limited space here, these will not be elaborated upon.

2.2.2 Other Organic SPEs

2.2.2.1 Polycarbonate-Based SPEs PEO-based SPEs were first mentioned by Wright et al. [76] and have recently experienced a renaissance. And although great efforts have been paid to compensate for the drawbacks of PEO-based solid electrolytes (extremely low ionic conductivity of 10^{-8} S cm^{-1}), tight coordination structures enabling strong coupling between Li-ion diffusion and segmental movements of polymer chains also need to be modified. Based on this, Koinuma et al. [104] synthesized aliphatic polycarbonates as novel hosts for SPEs through alternate copolymerization with carbon dioxide and epoxide. In addition, numerous aliphatic polycarbonate-based SPEs have been developed, such as PEC (polyethylene carbonate), PPC (polypropylene carbonate), PTMC (polytrimethylene carbonate). [105].

PEC can also be incorporated into alternating copolymers made up of carbon dioxide and epoxide in which a chain of (–O–(C = O)–O–) can be distinguished from the structure (Fig. 13) [106]. Based on this, Tominaga et al. [107] synthesized a novel composite of PEC and lithium bis(trifluoromethanesulfonyl)imide (LiTFSI) with appropriate ionic conductivity and high Li transference numbers in which the researchers reported that the ionic conductivity of PEC/LiTFSI became higher with increasing salt concentrations due to the imide anions from LiTFSI, which can cause plasticizing effects and enhance the segmental movement of the polymer chains. And as a result, the highest ionic conductivity obtained for the PEC/LiTFSI polymer electrolyte was 0.47 mS cm^{-1} at ambient temperatures and the Li-ion transference number was much larger than that of a PEO-based counterpart (0.4 and 0.1 for PEC and PEO, respectively) [108].

PPC is another biodegradable copolymer of propylene oxide and carbon dioxide that has attracted considerable interest [109–111], and the application of PPC-based SPEs in batteries is mainly focused on pristine PPCs and its copolymer SPEs. In addition, cellulose is widely considered to be one of the most ample and renewable resources bearing excellent properties, including outstanding thermal stability, chemical stability, environmental benignity and a high dielectric constant [112–115]. And based on the properties of these 2 materials, Cui et al. [116] developed a novel rigid-soft and high-performance polymer electrolyte

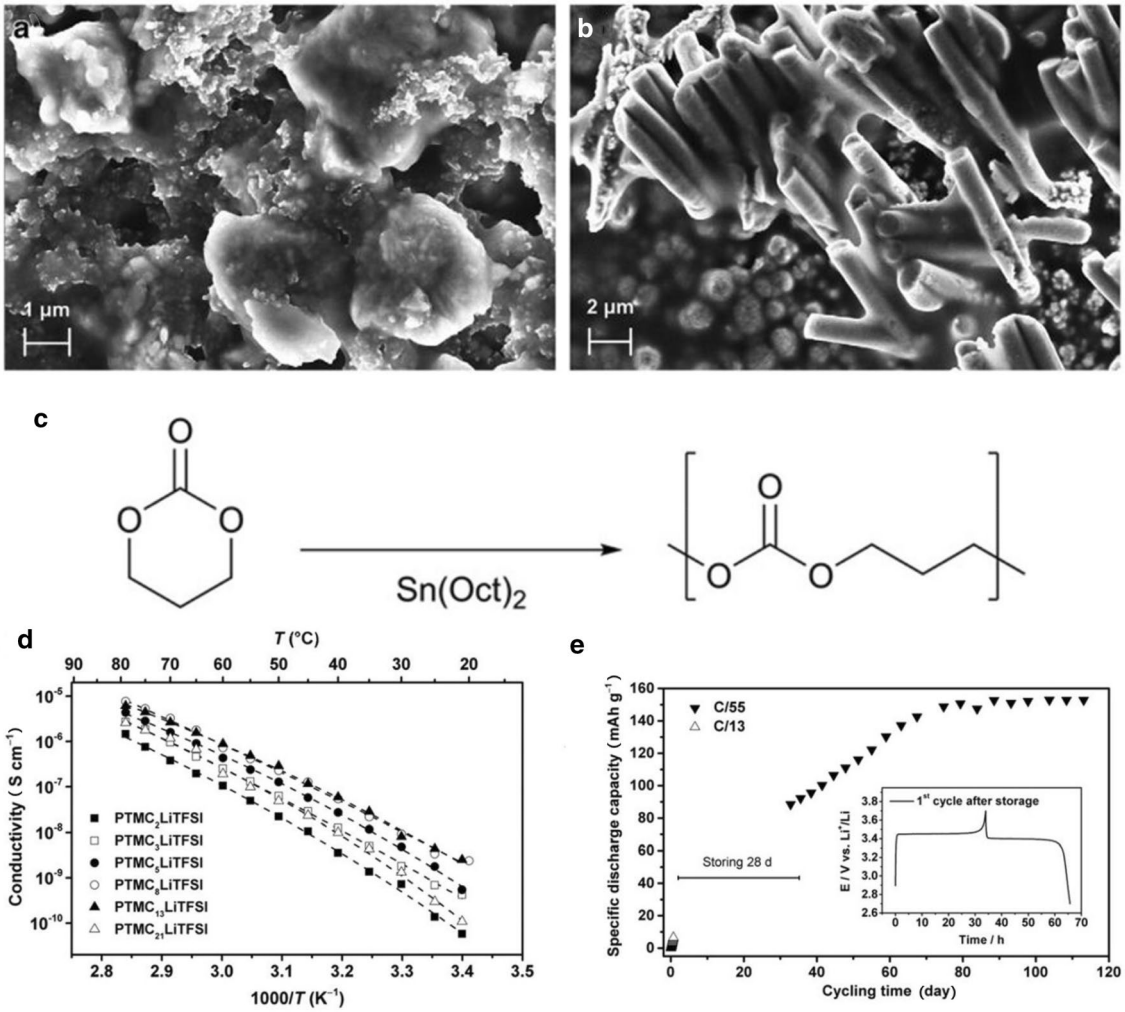

Fig. 13 SEM images of PTMC-LiTFSI materials with **a** $LiFePO_4$ composite electrode and **b** 3D Cu-nanopillar substrate. **c** Synthesis of PTMC. **d** Ionic conductivity of PTMC/LiTFSI materials as a function of temperature. **e** Diagram of the specific discharge capacities of a $LiFePO_4$/PTMC5LiTFSI/Li cell cycled at C/13 and C/55. Insert is the charge/discharge curve for the first cycle. Reprinted with permission from Ref. [117]. Copyright 2014 Elsevier

with nonwoven cellulose serving as the backbone and PPC transporting Li-ions in which the resulting safety-reinforced cellulose-PPC-LiTFSI SPE exhibited outstanding ionic conductivities, an appropriate electrochemical window and acceptable interfacial stability. Furthermore, $LiFePO_4$/Li and $LiFe_{0.2}Mn_{0.8}PO_4$/Li batteries using this cellulose-PPC-LiTFSI SPE showed extraordinary rate capabilities and cycling stability. These researchers also found an interesting phenomenon in which if a piece of the well-functioning cell was cut away, the remaining cell remained functional and could still light up a red LED lamp. Moreover, the safety of the cells using the cellulose-PPC-LiTFSI SPE also increased to unprecedented levels, providing a new avenue for the synthesis of high-voltage, ambient-temperature SPEs for LIBs.

Moreover, PTMC is also a new host material for SPEs that can be synthesized through the ring-opening polymerization of cyclic monomers (Fig. 13), through which a high-molecular-weight polymer serving as a base material for electrolytes can be obtained. Here, Sun et al. [117] reported that a $LiFeO_4$-based LIB using a homogenous mixture of PTMC and LiTSI can exhibit high discharge capacities and reach a specific plateau of 153 mAh g^{-1}. These researchers also reported that the ionic conductivity of this mechanically robust and flexible PTMC-based electrolyte can reach 10^{-7} S cm^{-1} at elevated temperatures and that it possessed good electrochemical stability, demonstrating the potential of PTMC in different battery applications.

2.2.2.2 Polysiloxane-Based SPEs In general, the development of oligo(ethylene oxide) polymers is considered to be

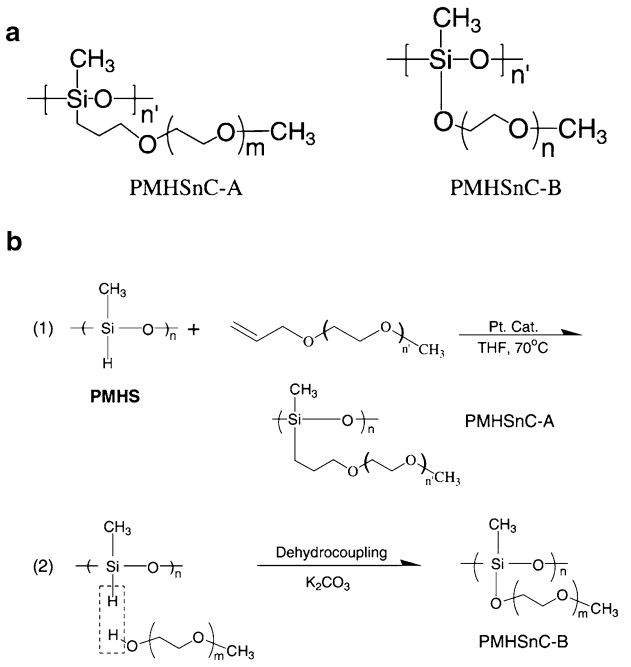

Fig. 14 **a** Chemical structures of mono-comb poly(siloxane-g-ethylene oxide). **b** Synthesis of mono-comb poly(siloxane-g-ethylene oxide). Reprinted with permission from Ref. [121]. Copyright 2003 Elsevier

a promising means to obtain amorphous polymers that are preferred for ideal SPEs and various polymer backbones have been studied [118]. Among these, polysiloxanes possess a very flexible backbone that can act as a potential host for polymers due to its low glass transition temperature, large free volume and good electrochemical stability [119] in which various organic groups can be connected to the silicon including ethylene oxide with side chains (chemical structure and synthesis of mono-comb poly(siloxane-g-ethylene oxide)). Despite the comparable conductivity for practical use, polysiloxane-based SPEs have been reported to possess low mechanical strength; however, this can be ameliorated through cross-linking or networking with polymers [25, 120]. In addition, several studies have investigated the ionic conductivity of polysiloxane-based SPEs based on the number and molecular weight of oligo(ethylene oxide) substituents and researchers have also developed comb-like poly(siloxane-*g*-ethylene oxide) as backbones for SPEs (Fig. 14). For example, Oh et al. [121] synthesized a $LiNi_{0.8}Co_{0.2}O_2$/SPEs/Li cell that exhibited exceptional cycling performances with negligible capacity decline, suggesting that polysiloxane-based SPEs can serve as potential candidates in large-scale battery applications. Fonseca et al. [122] also explored poly(dimethyl siloxane-co-ethylene oxide) (P(DMS-co-EO)) copolymers, and through AC impedance analysis they reported that the maximum ionic conductivity of the copolymer film with 5 wt% $LiClO_4$ can reach 2.6×10^{-4} S cm^{-1} at room temperature and that the electrochemical stability window was wide, suggesting that P(DMS-co-EO)/$LiClO_4$ electrolytes are promising in electrochemical devices.

Furthermore, Hooper et al. [123] proposed in 2011 the possibility that disubstituted polysiloxanes are superior to monosubstituted analogues in terms of electrochemical performance and synthesized a series of double-comb polysiloxane polymers with a growing number of ethylene oxide units in the side chains and reported improved ionic conduction performances as compared with mono-comb polysiloxanes.

2.2.2.3 Plastic Crystal-Based SPEs Novel approaches revolving around the core idea of dissolving salts into highly flexible plastic crystals have been adopted by many researchers [124, 125]. This is because plastic crystals are a class of materials with disordered structures and lattice defects resulting from rotatory motions of included globular-shaped cations and anions [125, 126], allowing for excellent properties such as greater plasticity and enhanced ionic conduction as compared with normal rigid crystals [127]. And among LIB electrolytes, nitrile materials have attracted great attention due to their high thermodynamic stability as well as their extraordinary electrochemical oxidation resistance [4] as a result of the strong interaction between nitrile functional groups (–C≡N) and Li^+ ions that can enhance the ionic conduction of nitrile-based SPEs [83]. Based on these factors, nitrile-based succinonitrile (N≡C–CH_2–CH_2–C≡N, SN) is a highly polar plastic-crystalline molecule that can dissolve various types of Li salts to achieve great ionic conductivity (two orders of magnitude above polymers) [125]. In addition, SN can maintain its plastic-crystalline phase in temperatures ranging from −40 °C to almost 60 °C (the melting point) [128].

Nevertheless, SN cannot be used as a self-standing film copolymer because it is extremely plastic and prone to deformation [25] and therefore is usually used as a versatile additive to obtain plastic crystal composite electrolytes (PCCEs) with enhanced ionic conductivity and robust mechanical properties. For example, Maier et al. [129] reported the feasibility of SN as an ionic conductivity enhancer in 3 polymer electrolyte systems, including PEO-LiTFSI, P(VdF-HFP)-LiTFSI and P(VdF-HFP)-LiBETI (LiBETI: lithium bisperfluoroethylsulfonylimide) in which the researchers attributed the enhanced ionic conduction to the strong solubility of SN for Li salts and the decreased crystallinity of the polymer. Lee et al. [127] also proposed a simple method to synthesize self-standing PCCEs through integration with UV (ultraviolet)-cured ethoxylated trimethylolpropane triacrylate (ETPTA) and SN-LiTFSI in which a transparent, nonsticky, and self-standing X-PCCE was synthesized

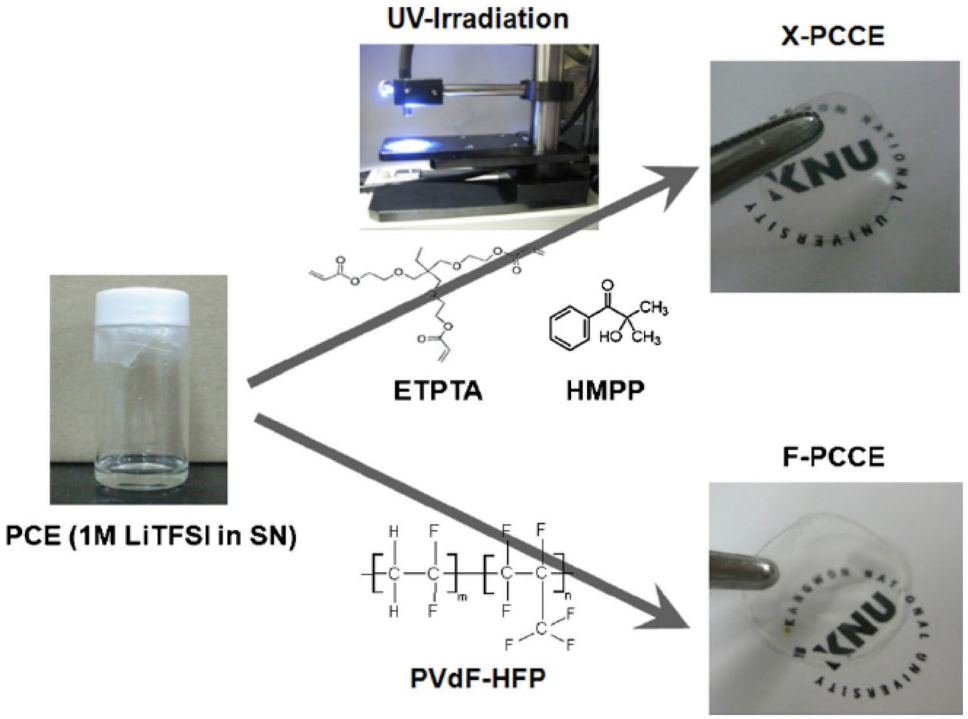

Fig. 15 UV curing process and images of the PCE, the X-PCCE and the F-PCCE. Reprinted with permission from Ref. [127]. Copyright 2011 Elsevier

after the trifunctional groups on an ETPTA monomer were cross-linked under exposure to UV lights for 20 s (Fig. 15). In addition, these researchers also synthesized F-PCCE through the integration of the conventional PCCE with polyvinylidenefluoride-co-hexafluoropropylene (PVdF-HFP) and reported that the resulting F-PCCE provided high ionic conductivity and unprecedentedly robust mechanical strength. Lee et al. [130] further fabricated a PCCE with a semi-interpenetrating polymer network (semi-IPN) as a matrix and a plastic crystal electrolyte (PCE, 1M lithium bis-trifluoromethanesulfonimide in succinonitrile) and reported unprecedentedly improved bendability and good ionic conduction, providing a novel method to fine-tune the electrochemical and physicochemical properties of PCCEs through anomalous UV-curable semi-IPN architectures as polymer matrixes.

2.3 Organic–Inorganic Hybrid SPEs

Organic–inorganic hybrid SPEs, including inert ceramic fillers (Al_2O_3, TiO_2, SiO_2, etc.), ferroelectric ceramic fillers ($LiNbO_3$, $PbTiO_3$ and $BaTiO_3$), clay and fast ion conductors [131–136], have also been reported to be promising in LIBs. In organic–inorganic hybrid SPEs, inorganic materials can be dispersed into polymer matrixes to effectively promote Li-ion conduction, create robust mechanical strength and provide more stable interfaces in SPEs [137–139]. The general idea of dispersing fine ceramic materials into ionic conductors has been prevalent since 1973 in which Liang et al. [140] proposed the feasibility of incorporating Al_2O_3 particles into Li salts to enhance Li^+ conduction. Here, the two-phase coexistence of ceramic fillers and ion conductive polymers has attracted considerable interest after observations of enhanced conductivity and interfacial stability as compared with ceramic-free systems. In addition, a series of studies have reported that the addition of ceramic fillers can inhibit the crystallization kinetics of PEO polymer chains, extend the amorphous regions and promote specific surface interactions [87, 131, 141]. Furthermore, Sun et al. [132] in their study measured the conductivity of composites made up of different ferroelectric ceramics ($BaTiO_3$, $PbTiO_3$ and $LiNbO_3$) and Li salts ($LiClO_4$, $LiBF_4$, $LiPF_6$, $LiCF_3SO_3$ and $LiN(CF_3SO_2)_2$) (Fig. 16) and rationalized that the improved conductivity was based on the association tendencies of anions with Li^+ and the spontaneous polarization of fillers from their particular crystal frameworks, resulting in substantially reduced interfacial resistances between electrolytes and electrodes. Murugan et al. [142] also proposed a novel polymer electrolyte of poly(ethylene) glycol (PEO) complexed with $SrBi_4Ti_4O_{15}$ fillers and $LiClO_4$ and used the citrate gel technique to form the same ferroelectric fillers with particle sizes that were much smaller than that of the conventional method and reported that the reduction in the particle size of fillers can lead to better ionic conduction.

In addition, Croce et al. [141, 143] utilized inert ceramic fillers (SiO_2, Al_2O_3, TiO_2, etc.) to develop nanosized PEO-based polymer electrolytes with improved properties and reported that among the inert materials, TiO_2 was the most promising in the improvement in ionic conduction due to the fragile connection between Li^+ ions and polymer chains

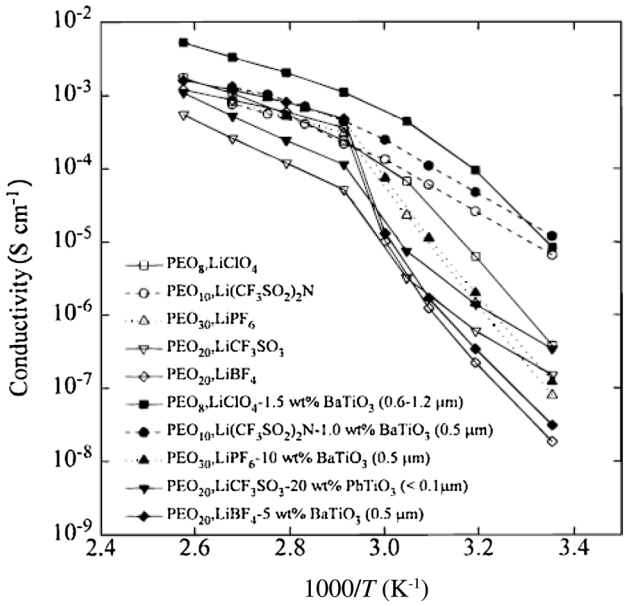

Fig. 16 Conductivity of composites consisting of ferroelectric ceramics, Li salts and PEO. Conductivity values were evaluated during the first heating scan by using impedance spectroscopy measurements. Reprinted with permission from Ref. [132]. Copyright 2000 The Electrochemical Society

[25]. Lin et al. [144] also found that the reduction in TiO_2 grain size can increase the ionic conductivity of nanosized TiO_2-modified composite polymer electrolytes (CPEs) and that there was a great dichotomy in the ionic conduction between PEO-10% $LiClO_4$-5% TiO_2 (3.7 nm) and pure PEO-10% $LiClO_4$ in which the value of the former was an order of magnitude larger than that of the latter. Furthermore, these researchers also reported that transference numbers of 0.51 and 0.21 were achieved for the TiO_2-modified CPE and pure PEO-$LiClO_4$. Researchers have also reported that the interaction between TiO_2-doped Li salts and PEO chains can promote structural modifications and endow Li-ions with favorable migration pathways [139] and that the high mobility of charge carriers can be regarded as the result of the interactions of polymers in the amorphous region even at ambient temperatures.

Montmorillonite (MMT) as a layered clay with a lamellar shape has attracted intense interest from researchers in the development of polymer–clay electrolytes due to the fact that lamellar elements can exhibit high in-plane strength, high aspect ratio and stiffness [145]. For example, Zhang et al. [146] reported that PEO/MMT/LiTFSI solid polymer electrolytes demonstrated reinforced Li-ion conductivities in which an optimal electrolyte composed of 10 wt % MMT reached a conductivity of 3.22×10^{-4} S cm^{-1} at 60 °C and a corresponding solid-state battery displayed good cycling stability and an acceptable discharge capacity of 643 mAh g^{-1} under the same conditions.

Carbon nanotubes (CNTs) are widely thought to be ideal polymer matrixes to reinforce mechanical properties through high aspect ratios, good strengths and modulus. In addition, CNTs possess rich electron clouds that can create strong affinity with Li-ions and facilitate Li salt dissociation as well as ion migration through the framework [147, 148]. However, the electrical shorting of CNTs greatly restricts practical production. As an example, Tang et al. [149] successfully assembled hybrid 3D nanofillers with 1D CNTs and 2D MMT clay platelets (Fig. 17) and reported that the Li-ion conductivity and tensile strength of PEO-$LiClO_4$ electrolytes with the synthesized nanofiller were greatly improved, demonstrating the feasibility of embedding conducting–insulating hybrid materials in the synthesis of desirable SPEs.

Fast ionic conductors also possess many extraordinary merits, such as the lack of solution leakage, environmental benignity, nonflammability, high thermal stability, good electrochemical properties. [150]. Because of this, Murugan et al. [83] synthesized cubic $Li_7La_3Zr_2O_{12}$ (LLZO) with a garnet-like structure and Lee et al. [151] synthesized organic–inorganic membranes consisting of PEO and the diverse tetragonal LLZO content in which through AC impedance measurements, 52.5% LLZO was confirmed to be able to provide an optimal ionic conductivity of 4.42×10^{-4} S cm^{-1} at 55 °C. Here, these researchers suggested that the hybridization of inorganic and organic materials can create synergetic effects to improve ionic conductivity in which the charge/discharge test of Li/composite membrane/$LiNi_{0.6}Co_{0.2}M_{0.2}O_2$ was more satisfactory than that of PEO-only materials and a counterpart material with 52.5% Al_2O_3, demonstrating the viability of all-solid organic–inorganic hybrid composite membranes. Despite this, further studies into these hybrids should be devoted to the improvement in cycling performances for practical battery systems.

3 Factors Influencing the Ionic Conductivity of Solid-State Electrolytes

The ionic conductivity of solid-state electrolytes is a key parameter to determine electrochemical performance; however, few possess acceptable intrinsic conductivity. Based on this, great efforts have been put into the enhancement of ionic conductivity in solid-state electrolytes. Here, the understanding of the mechanisms and influences of ionic conductivity in solid-state electrolytes is the key, and therefore, this section will introduce relevant research based on 3 aspects of solid-state electrolytes, including structure, composition and the interphase.

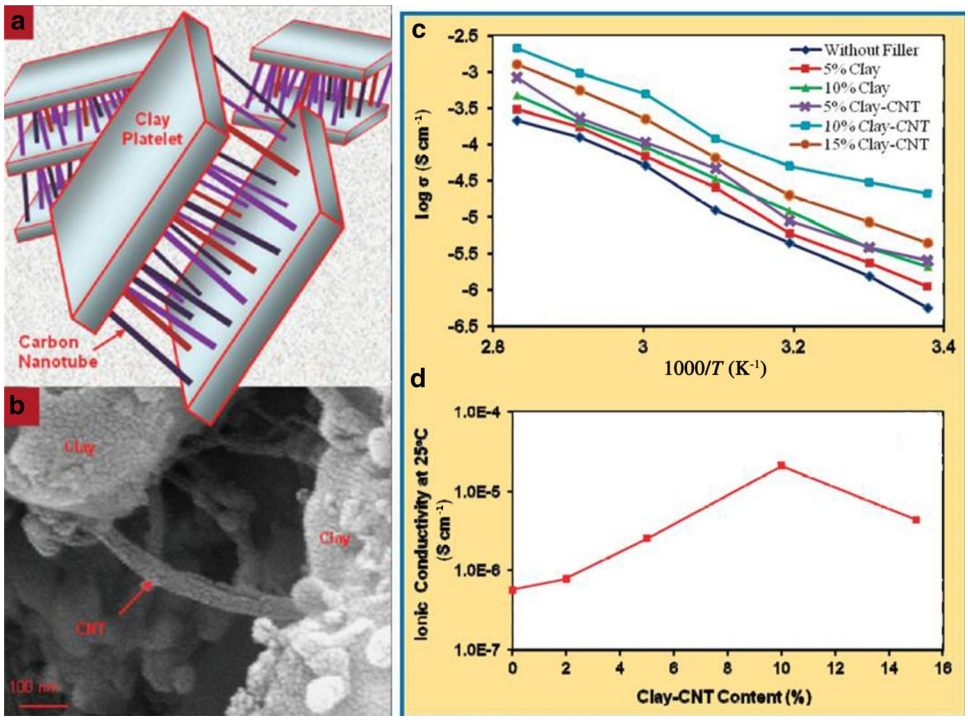

Fig. 17 **a** Schematic of montmorillonite. **b** SEM image of clay-CNT hybrid fillers. **c** Ionic conductivities of pure PEO and composites at different temperatures. **d** Ion conductivities of PEO composites at 25 °C with diverse hybrid filler content. Reprinted with permission from Ref. [149]. Copyright 2012 American Chemical Society

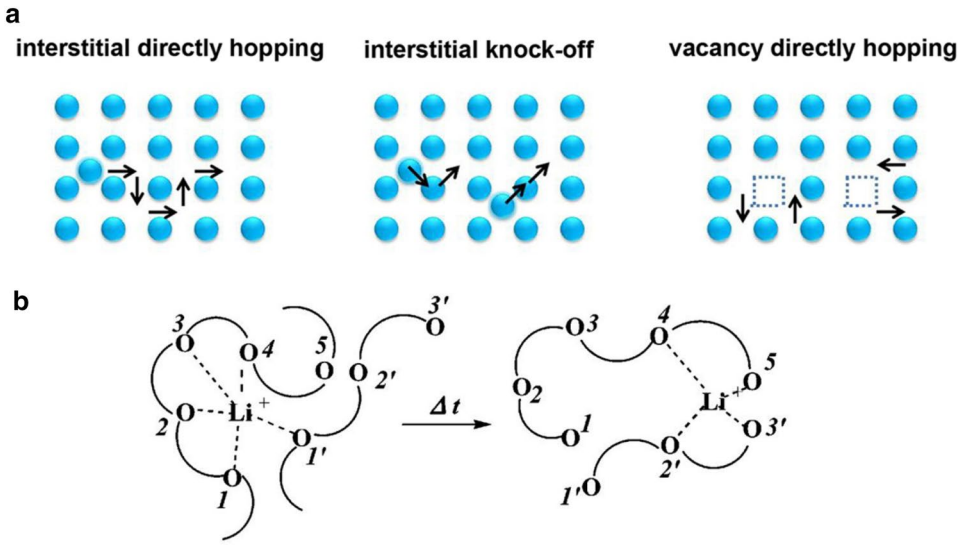

Fig. 18 Schematic of Li-ion transport in **a** crystalline and **b** polyether media. Reprinted with permission from Ref. [152]. Copyright 2004 American Chemical Society

3.1 Structure

The mechanism and conductivity of ionic transport are closely related to crystal structure and vary greatly for different systems. In general, there are 3 Li^+ diffusion mechanisms in inorganic solid electrolytes, including interstitial direct hopping, interstitial knock-off and vacancy direct hopping (Fig. 18) [153] and a thorough comprehension of ionic transport is imperative to remold and design optimal solid electrolytes. For example, Ceder et al. [72] reported that frameworks with a body-centered cubic (bcc) anion arrangement that possess lower activation barriers are superior to other anion packing models (fcc, hcp) and can achieve optimal ion transfer rates. Overall, the conductivity of ions in crystalline structures follows the Arrhenius law as follows:

$$\sigma_{DC}T = A_{\sigma}\exp(-E_{\sigma}/k_{B}T) \quad (1)$$

However, for structures that are not in a long-range order (*i.e.,* glass, polymers or crystalline materials with randomly occupied defects), the conductivity of ions does not follow the linear Arrhenius law and can be better represented by the Vogel–Fulcher–Tammann (VFT) or Williams–Landel–Ferry (WLF) equations as follows [154]:

$$\sigma_{DC}T \propto A_{\sigma}\exp[-E_{\sigma}/k_{B}(T-T_{0})] \quad (2)$$

in which in crystalline inorganic solid electrolytes, defect sites may weakly impact each other, whereas for amorphous systems with many defects, the correlation between mobile ions and the interaction between Li^+ and framework ions should be taken into consideration [155]. And until now, no explicit theories into ion diffusion behaviors in disordered systems have been proposed; however, a few amorphous solid electrolytes have been reported to show higher ionic conductivities than crystalline or rigid solid electrolytes in laboratory settings in which the improvements may be due to the vast defects in the amorphous materials. In addition, researchers have also reported that the mixing of crystalline materials with amorphous glass can also enhance conductivity, which may be attributed to greater defects around the crystalline region [26].

As for SPEs, it is generally accepted that ions move mainly in the amorphous phase [156] in which the motion of ions in polymer systems is closely related to the structural relaxation of polymeric chains. For example, Ratner et al. [157] studied Li-ions coordinated with polar groups in polymer chains (Fig. 18) and reported that accompanying the continuous peristalsis of segments, polar groups that are solvated by Li-ions can be replaced to create the incessant movement of Li-ions, demonstrating that the number and stability of polar groups as well as the chain strength and peristalsis of the polymer host all affect the conductivity of SPEs.

As for inorganic–organic composite electrolytes, multiphase structures can increase the complexity of the ion transport process in which both amorphous and crystalline components can provide access to ion transport to diversify pathways and the structure and distribution of different phases can make the process even more viable. Researchers have also reported that the introduction of nanosized inorganic components to polymers can enhance mechanical strength and ionic conductivity in which numerous researchers have reported the occurrence of Li-ion hopping near polyether–filler interfaces [158, 159]. Moreover, Wieczorek et al. [160] used structural characterizations obtained from FT-IR, NMR, DSC and EDX methods to propose an ionic transport mechanism in composite polymeric systems in which they demonstrated that the formation of various complexes near polyether–filler interfaces as a result of acid–base reactions is responsible for conductivity enhancements. And based on NMR, ac conductivity spectra and powder X-ray patterns results, Liu et al. [161] proposed a suppositional ionic conductivity mechanism for highly crystalline polymer electrolytes in which polymer molecules remained stationary whereas Li-ions hopped between adjacent units driven by defects and cavities in the crystalline phase, suggesting that larger crystallite sizes with more abundant defects can enhance ionic transport.

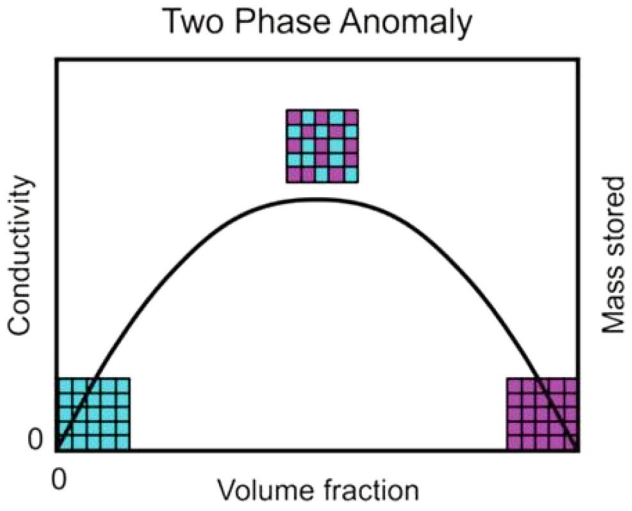

Fig. 19 Qualitative diagram of the enhanced conductivity and higher storage capacity of two-phase composites. Reprinted with permission from Ref. [166]. Copyright 2007 Elsevier

3.2 Composition

Initial research into ion transport systems was mainly focused on bulk properties; however, researchers soon realized that boundary layers are fundamentally connected with significant impact on ionic conduction properties in which Liang et al. reported in 1973 that two-phase LiI-Al_2O_3 possessed unusually high ionic conductivity in comparison with single-phase LiI. Since this study, serious research has been conducted into these solid electrolytes (referred to as "composite electrolytes" or "heterogeneous electrolytes") with Wagner et al. making significant contributions. Here, it is commonly believed that the improved conductivity of these solid electrolytes arises from the interfacial zones in which different compositions can bring about different interfaces with different conductive mechanisms [162]. Wagner et al. [163] further proposed that enhanced conductivity may originate from multiple reasons, including space-charge layers (SCLs), more intensive dislocation densities and the formation of new phases. Here, the SCL theory can be further referred to in publications by Maier et al. [162, 164, 165] and is universally approved and accepted (Fig. 19).

3.3 Dimension

The interface represents a discontinuity of the structure and usually arises simultaneously with variations in charge carrier concentration. In addition, interfacial regions can expand by reducing particle sizes or dimensions (i.e.,

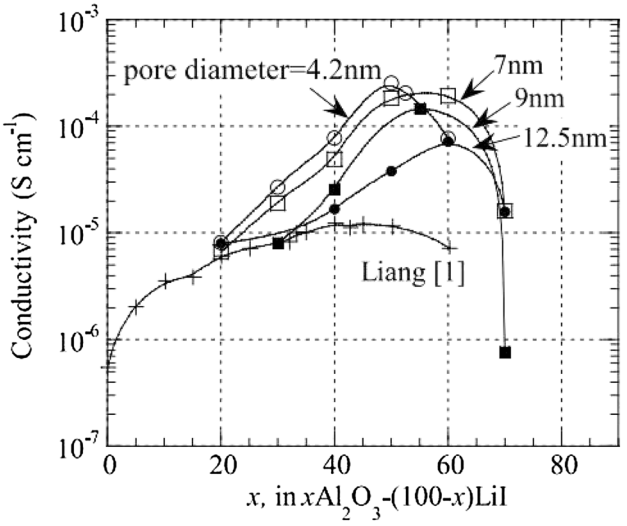

Fig. 20 Composition and pore size correlations with dc conductivity for Al_2O_3-LiI composites. Reprinted with permission from Ref. [167]. Copyright 2004 Elsevier

nanocrystallization) and in comparison with bulk materials, nanosized solid electrolytes possess much larger interfacial regions to allow for significantly enhanced ionic conductivity. Maekawa et al. [167, 168] also conducted research into the influence of Al_2O_3 pore sizes in composite electrolytes to improve ion conductivity and reported that conductivity can be greatly improved by 10–50-folds with the reduction in particle size. Here, the researchers suggested that this enhancement originated from overlapping space charges and the formation of new components in the interfacial region. In addition, Maier et al. [169] also proposed the possibility of the generation of metastable subsystems in the interface, and more detailed discussions can be found in their published literature. Overall, due to the introduction of enormous interfaces, the ionic conductivity of solid electrolytes has been significantly advanced through nanocrystallization, and therefore, this "nanoionics" is vital for future research (Fig. 20).

4 Advanced Characterization Techniques for the Study of Solid-State Electrolytes

In addition to traditional characterization techniques such as X-ray diffraction (XRD), energy dispersive X-ray detection (EDX), X-ray photoelectron spectroscopy (XPS), scanning electron microscopy (SEM), transmission electron microscopy (TEM), up-to-date and advanced techniques have emerged recently in the analysis and detection of solid-state electrolytes. Based on this, this section will introduce some of the latest techniques reported.

4.1 Time-of-Flight Secondary Ion Mass Spectroscopy

The interphase between electrode materials and solid-state electrolytes plays a definitive role in overall performance. Therefore, meticulous surface characterization by using powerful tools to confirm chemical changes is imperative. Here, time-of-flight secondary ion mass spectroscopy (TOF-SIMS) is a powerful characterization technology that possesses the ability to probe the composition, spatial distribution and structure of samples in which vast quantities of information can be obtained within a short period of time through high-quality spectra and direct chemical imaging. As a result, the high sensitivity and adaptability of TOF-SIMS have aroused increasing interest in application for material characterization. For example, Park et al. [27] studied the interface between $LiCoO_2$ and LLZO. Through the use of TOF-SIMS, they were able to obtain a 3D high-resolution elemental distribution mapping in which colored dots represented various elements with ionic concentrations shown based on color scales (Fig. 21). And as a result, these

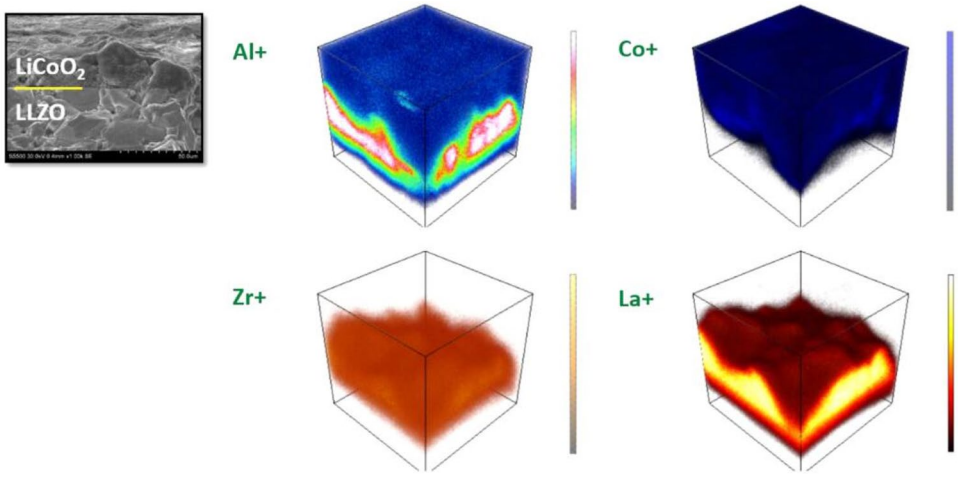

Fig. 21 3D elemental distribution graphs of the interface region of $LiCoO_2$/LLZO as acquired by TOF-SIMS. Reprinted with permission from Ref. [27]. Copyright 2016 American Chemical Society

researchers were able to observe that at the $LiCoO_2$/LLZO interface, Co diffused across the interface from $LiCoO_2$ into LLZO whereas Zr/La in LLZO diffused into $LiCoO_2$. In addition, these researchers also unexpectedly observed the results for Al, with Al diffusing over long distances and even at the end of $LiCoO_2$. These researchers also used XRD and TEM to confirm that this leach out of Al in LLZO can further cause the transformation of cubic LLZO into a tetragonal phase. Overall, due to its nondestructive testing and high sensitivity, TOF-SIMS will become more versatile in the field of electrochemistry.

4.2 Solid-State NMR Techniques

Solid-state nuclear magnetic resonance spectroscopy (SS NMR) is a critical and requisite characterization method for the detection of atomic level local structures and ion motions of specific species. In addition, various NMR techniques including pulsed-field gradient (PFG) NMR, triple-quantum MAS (3QMAS), magic angle spinning (MAS) NMR, spin–lattice (SLR) NMR, 3D exchange (2D EXSY) NMR and spin alignment echo (SAE) NMR have been employed and more often are combined to trace structural evolutions, ion diffusion pathways and ion conductor dynamics. This is because NMR techniques are nondestructive, non-contact and possess a wide range of applications toward not only crystalline but also amorphous materials. For example, Arbi et al. [170] explored $Li_{1+x}Al_xM_{2-x}(PO_4)_3$ materials (M = Ti, Ge) using MAS-NMR to ascertain ion locations and Li-ion diffusion pathways in which ^{27}Al and ^{31}P MAS-NMR as well as the spectra of ^{7}Li (Fig. 22) were investigated. Here, the researchers reported that the spectra were observed to be centered at ~0 ppm, which can be attributed to Li^+ at M1 and M3 sites with further fitting results of the spectra revealing that the quadrupole interactions at the M3 sites were significantly lower than that at the M1 sites, demonstrating enhanced Li^+ mobility at the M3 sites. In another study, Wang et al. [171] investigated the doped garnet-type solid electrolyte $Li_7La_3Zr_2O_{12}$ to reveal the influence of aliovalent substitution on ionic conductivity using high-resolution NMR analysis and found that the Li^+ ions had 3 sites in the garnet-type electrolyte, including 24*d* (tetrahedral sites), 48*g* and 96*h* (octahedral sites). Here, the researchers carried out 2D chemical exchange experiments using NMR to obtain a 2D ^{6}Li-^{6}Li exchange spectrum of $Li_{7-2x-3y}Al_yLa_3Zr_{2-x}W_xO_{12}$ (Fig. 23) in which the cross-peak at $\omega_1 = 0.8$, $\omega_2 = 1.6$ ppm revealed the close relationship between the 96*h* and 24*d* sites, supporting Li migration along 24*d*–96*h*–48*g*–96*h*–24*d*. Liang et al. [172] also used diverse SS NMR techniques to investigate the origins of the optimal Li-ion conductivity in $Li_{10}GeP_2S_{12}$ (LGPS) solid electrolytes and found that Li-ions in LGPS systems can diffuse along 1D tunnels simultaneously with 2D plane pathways, which

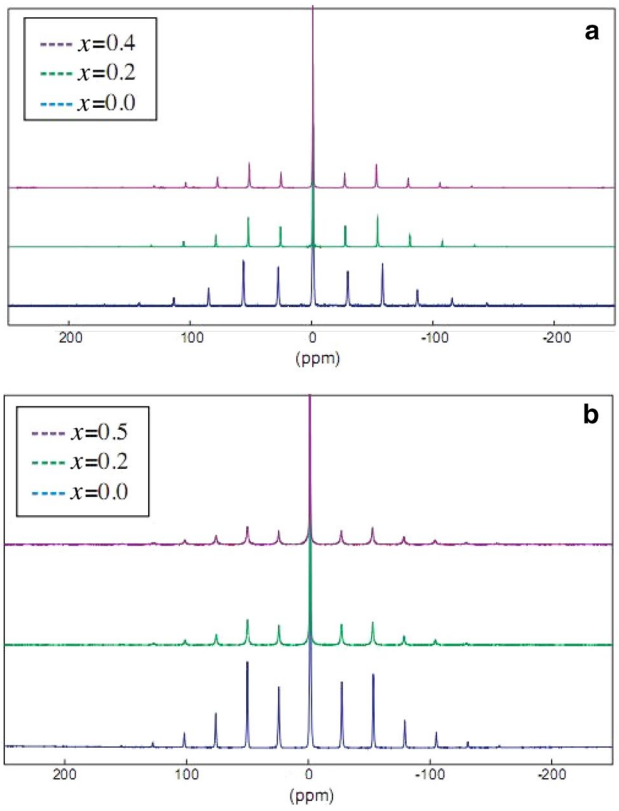

Fig. 22 ^{7}Li MAS-NMR spectra of **a** LATP and **b** LAGP samples. Reprinted with permission from Ref. [170]. Copyright 2015 Elsevier

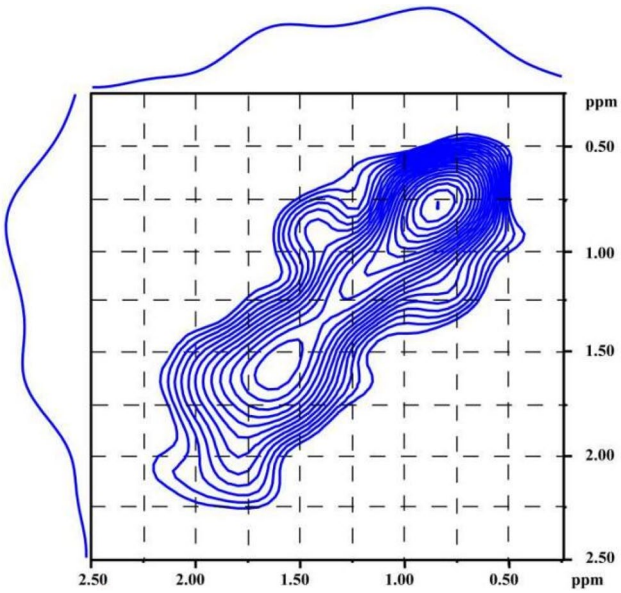

Fig. 23 ^{6}Li-^{6}Li exchange spectra of $Li_{7-2x-3y}Al_yLa_3Zr_{2-x}W_xO_{12}$. Reprinted with permission from Ref. [171]. Copyright 2015 American Chemical Society

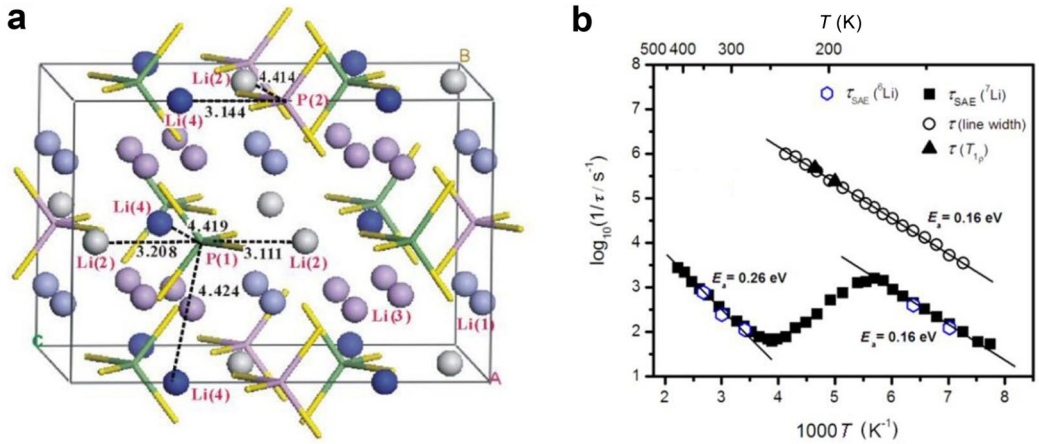

Fig. 24 **a** Crystal structure diagram of LGPS. **b** ^{7}Li $1/\tau$ of LGPS, ^{7}Li spin-lock SLR NMR and the line width. Reprinted with permission from Ref. [172]. Copyright 2015 American Chemical Society

corresponded to activation energy of 0.16 eV and 0.26 eV, respectively. In addition, these researchers obtained the relationship curve of $1/\tau_{SAE}$ versus the reciprocal of temperature for LGPS (Fig. 24) in which τ_{SAE} is a parameter denoting the correlation time of Li^+ migration based on Eq. (3) and found that τ_{SAE} experienced an initial decline followed by an upsurge and subsequent decline with rising temperatures, suggesting the existence of 2 different processes for Li-ion diffusion in LGPS systems. Furthermore, based on the 2 gradients of the Arrhenius curve in the low- and high-temperature areas, activation energy of 0.16 eV and 0.26 eV can be obtained. For a more detailed reference, Xiang et al. [173] provided a detailed overview of NMR techniques utilized in the solid electrolyte field.

$$S_2\left(t_m, t_p\right) = \left\{A \exp\left(-\frac{t_m}{\tau_{SAE}}\right) + B\right\}^{\gamma_c} \exp\left(-\frac{t_m}{T_{1Q}}\right) \quad (3)$$

4.3 Magnetic Resonance Imaging

Magnetic resonance imaging (MRI) is an up-and-coming technology in the fields of catalysis [174, 175], polymers [176], corrosion [177], fuel cells [178], etc, due to its high reliability and nondestructive testing. And recently, studies using MRI have been emerging in the area of batteries to provide both quantitative and spatial information. For example, Chien et al. [177] used 2D and 3D ^{7}Li MRI to study Li distribution in the solid electrolyte $Li_{10}GeP_2S_{12}$ and found Li deficiency at the interface and enhanced heterogeneity of Li distribution through repeated charge and discharge in which quantitative 3D ^{7}Li MRI images of $Li_{10}GeP_2S_{12}$ and PEO-coated $Li_{10}GeP_2S_{12}$ pellets after cycling (Fig. 25) showed significant Li depletion on the top and bottom layers with Li depletion being more severe at the top whereas none was observed in the bulk. In addition, these researchers analyzed the scattering of histograms and found that the Li content for both top and bottom layers was heterogeneous in the unmodified sample whereas with the modification of the PEO film at the interface, Li loss and the heterogeneity distribution of Li were dramatically reduced. Romanenko et al. [28] also conducted in situ MRI studies of organic ionic plastic crystals (OIPCs) in a solid-state battery with a focus on Li^+ transport at the interface and proposed the relationship between the ^{1}H MRI signal and Li-ion content/distribution through the use of a novel SPRITE (single-point ramped imaging with T_1 enhancement) technique in which the displacement of the front electrolyte, a fast grain boundary transfer and Li^+ exhaustion at the interface were detected.

5 Promising Strategies to Enhance Li-Ion Transport

5.1 Structural Tuning

5.1.1 Tuning lattice Volume Through Substitution

For crystalline electrolytes, incremental lattice volumes can result in higher Li-ion conduction and lower activation energy in which lattice volumes can be changed through 2 effective approaches including substitution and mechanical strain. In terms of substitution, increased ionic conductivity can be achieved through iso-valent substitution in a given structural framework to determine lattice volumes and bottleneck sizes for Li-ion diffusion. For example, the conductivity of NASICON-type $LiM_2(PO_4)_3$ (M = Ge, Zr or Ti) can be enhanced through elemental substitution to

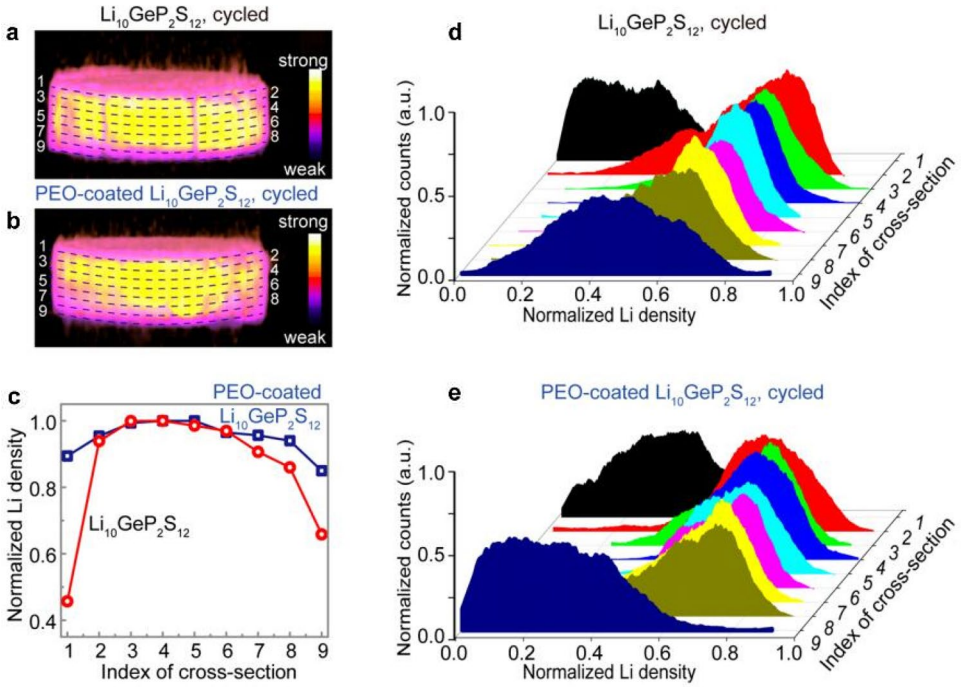

Fig. 25 **a, b** ^{7}Li 3D MRI images of cycled $Li_{10}GeP_2S_{12}$ pellets with and without PEO coating. **c** Plot of normalized ^{7}Li densities versus the layer index. **d, e** Bar graphs of normalized Li counts at different depths corresponding to **a**, **b**. Reprinted with permission from Ref. [179]. Copyright 2018 American Chemical Society

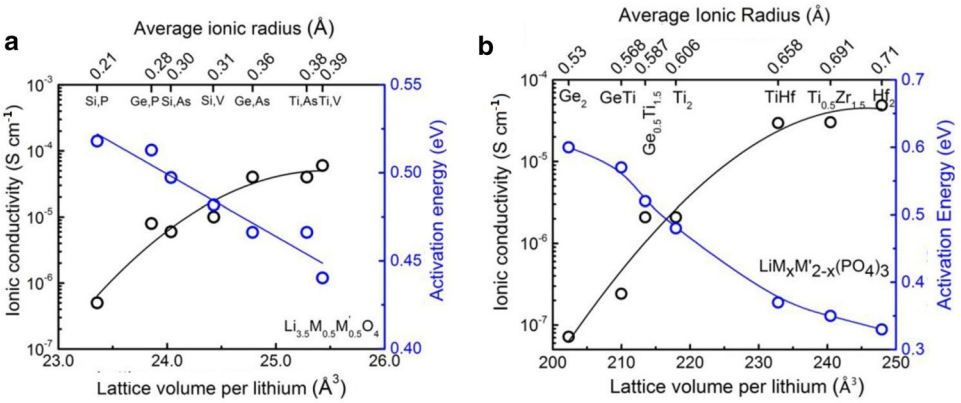

Fig. 26 Li-ion conductivity of **a** LISICON-like $Li_{3.5}M_{0.5}M'_{0.5}O_4$ and **b** NASICON-like $LiM_xM'_{1-x}(PO_4)_3$ as a function of lattice volume per Li atom. Reprinted with permission from Ref. [180]. Copyright 2016 American Chemical Society

generate $Li_{1+x}M_xTi_{2-x}(PO_4)_3$ (M = Al, Cr, Ga, Fe, Sc, In, Lu, Y or La) (Fig. 26) [181]. In addition, aliovalent substitution of O^{2-} with S^{2-} in the sulfide electrolyte Li_3PS_4 can form the thio-LISICON compound $Li_{10}GeP_2S_{12}$ (LGPS) and improve Li-ion conductivity through the enlargement of ion transport channels [182]. As for perovskite-type structures with a formula of ABO_3 (A = La, Sr, or Ca; B = Al or Ti), substitutions with larger size A-site rare-earth metal ions (Sm < Nd < Pr < La) can also enlarge lattice volumes and improve Li-ion conductivity and lower activation energy [183]. Furthermore, enhanced Li-ion conductivity induced by substitution was also reported for LISICON-type electrolytes [184].

Aside from substitution, mechanical strain can also alter lattice volume through tensile or compressive strain on crystalline conductors in which according to DFT studies on cubic $Li_7La_3Zr_2O_{12}$ (cLLZO) [185] and LGPS [186], isotropic compressive strain can significantly lower Li-ion conductivity whereas tensile strain showed no effects. This suggests that the further increase in lattice volume has little effect on the reduction in Li-ion activation energies when transiting bottleneck points or the lattice volume of these 2 conductors is close to optimization. Recent studies have also demonstrated that the tailoring of Li conductivity is attainable through the generation of strain from lattice mismatches in the substrates of thin-film growth of Li-ion conductors with $Li_{0.33}La_{0.56}TiO_3$ thin films grown on $NdGaO_3$ (NGO) being a good example [187, 188] in which the distinct strain imposed by NGO along the *a*- and *b*-axes directions can lead to the anisotropy of the ionic conductivity. Despite these results, however, more efforts are needed to deeper probe into the implications

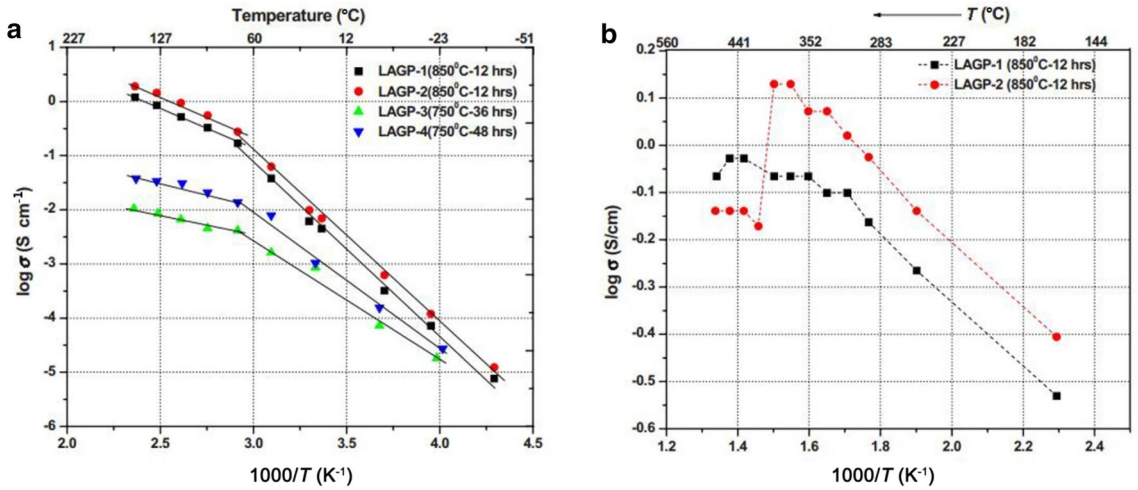

Fig. 27 **a** Arrhenius plots of the conductivity of LAGP specimens crystallized at diverse temperatures and times. **b** Arrhenius plots of the conductivity of LAGP specimens crystallized in the high-temperature region. Reprinted with permission from Ref. [196]. Copyright 2009 The Electrochemical Society

of mechanical strain on Li-ion conduction with considerations of the negligible variations in ionic conductivity.

5.1.2 Decreasing Grain Boundary Resistances Through the Control of the Space-Charge Effect

Decreasing grain boundary resistance is another attractive approach to increase Li-ion conductivity, and researchers have reported that significant decreases can be achieved through the incorporation of other phases at the grain boundary as caused by the space-charge effect [189]. Here, 2 separate processes have been adopted to create new phases at interfacial boundaries in which the first involves additive fillers. This is because additive fillers can play an important role in enhancing conductivity in which in addition to conventional ionic transport in liquid electrolytes, Li-ion adsorption on filler particles can lead to increased vacancy concentrations of Li-ions in space-charge regions, contributing to higher conductivities. For example, Cao et al. [190] reported that polymer electrolytes can show high ionic conductivity due to well-dispersed filler nano-TiO_2 particles in the conductor. And based on C-rate and AC impedance analysis, these researchers proposed that the interfacial resistance of the cells can be decreased due to ionic mobility in the vicinity of TiO_2 nanoparticle boundaries. Furthermore, more favorable Li-ionic conduction pathways can be created through Lewis acid–base interactions or through the formation of favorable transport processes closely connected to TiO_2 nanoparticles [136, 191]. For example, Kumazaki et al. [192] reported that the grain boundary resistance of garnet-structured $Li_7La_3Zr_2O_{12}$ can be lowered through the incorporation of Si and Al and attributed this to the interface of amorphous Li-Al-Si-O as well as to the nanocrystalline $LiAlSiO_4$ that can improve Li-ion migration between $Li_7La_3Zr_2O_{12}$ grains. Moreover, the addition of B_2O_3, TiO_2 and ZrO_2 has also been reported to be able to promote the rearrangement of grains to lead to better connections during the crystallization process [193–195].

The second process to create new phases at interfacial boundaries is a sintering process that does not require fillers and can provide conductive phases to enhance Li-ion conductivity. For example, Kumar et al. [196, 197] reported that during the synthesis of LAGP, the formation of Li_2O and $AlPO_4$ at the grain boundaries can result in space-charge-mediated effects on conductivity in which the effects displayed in the LAGP specimens were attributed to their impact on activation energy. Here, the researchers reported that the formation of $AlPO_4$ at ~ 70 °C showed small space-charge effects as reflected in the Arrhenius plot whereas the formation of Li_2O at ~ 400 °C contributed to significant drops in conductivity (Fig. 27), allowing the formation of Li_2O:Li^+ complexes to display enhancements in ionic conductivity. And aside from synthesis temperatures, these researchers also reported that the concentration of dielectric phases can also influence space-charge effects [196].

Moreover, ambient conditions and preparation methods can also affect the performance of grain boundaries. For example, Kali et al. [198] proposed that spark plasma sintering can impart desirable properties such as fast densification, minimization of coarse particles and fine grain-to-grain bonding in which $Li_7La_3Zr_2O_{12}$ sintered in Ar atmosphere displayed lower Li-ion conductivity due to fewer grain boundaries as compared with that prepared in air [199].

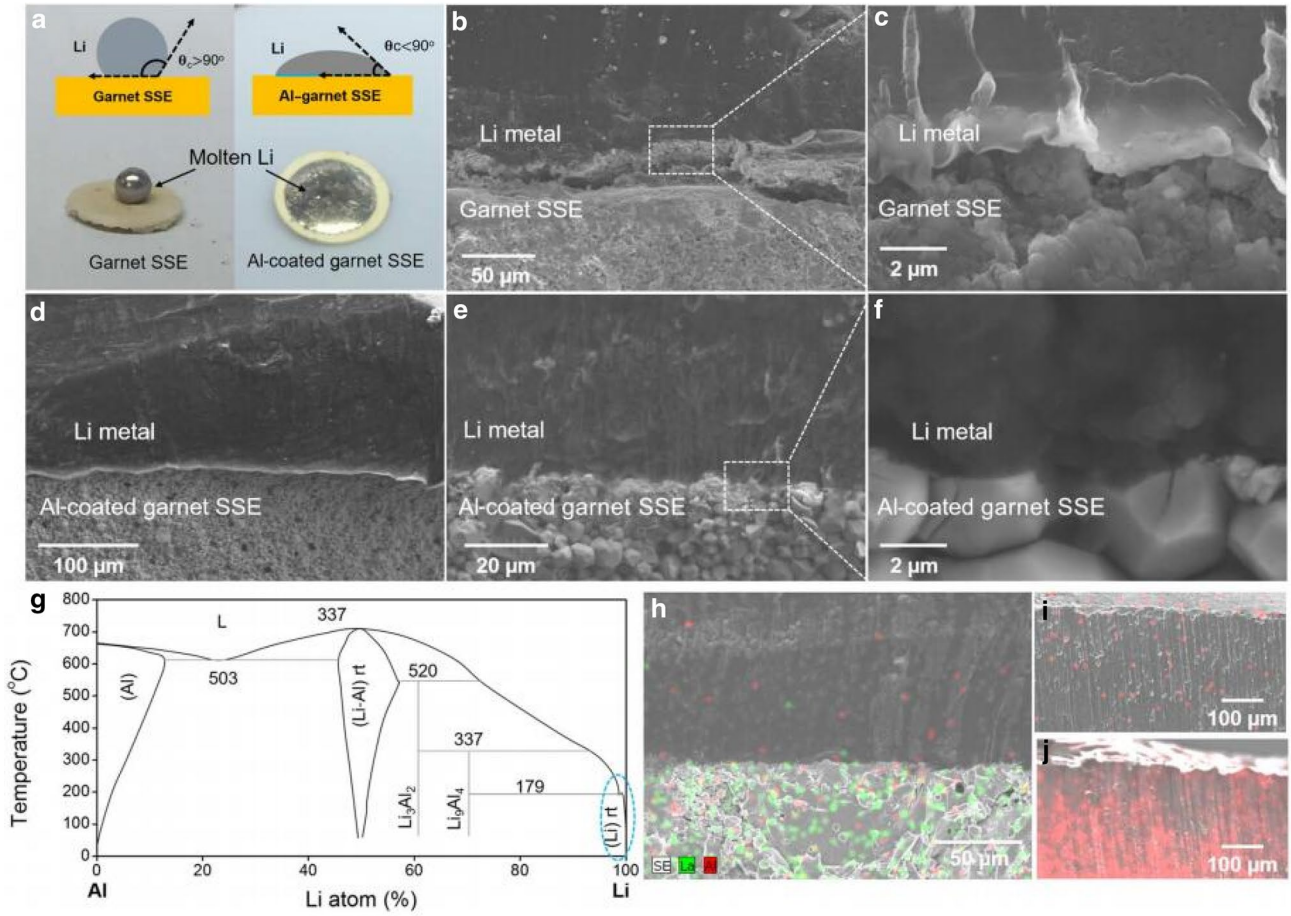

Fig. 28 **a–f** Wetting properties and appearances of interfaces between bare and Al-coated LLZO and Li. **g** Phase diagram of Li-Al. **h** Elemental mapping of the cross section. **i, j** Elemental mapping of the top area of Li. Reprinted with permission from Ref. [200]. Copyright 2017 Science

5.2 Interface Engineering

Different from common batteries or semisolid batteries, solid-state batteries are composed of solid materials in which a prominent solid–solid interface barrier occurs between the electrolyte and electrodes, making ion diffusion sluggish. In addition, the gaps between the electrolyte and electrodes can also impair battery cycling ability or render them inoperable. Therefore, sufficient contact and the more important issues of good electrochemical compatibility and fast interfacial ionic transfer between electrodes and electrolytes are the key to the future application of solid-state electrolytes. Based on this, this section will present related studies on this topic.

5.2.1 Interface Between the Electrolyte and the Anode

Garnet-type $Li_7La_3Zr_2O_{12}$ (LLZO) solid electrolytes are promising materials for next-generation batteries due to remarkable intrinsic conductivity and stability toward Li anodes. However, a poor interfacial wetting ability limits further application as a result of insufficient physical contact. To address this, Hu et al. [200] proposed the physical deposition of an Al layer as thick as 20 nm using Ebeam evaporation to form a Li-Al alloy at the interface between LLZO and Li (Fig. 28). Here, the researchers reported that the as-formed artificial alloy layer can enable the wetting of the LLZO surface to allow the interface resistance to be significantly reduced from 950 to 75 Ω cm^2. In addition, these researchers also reported that this electrode design showed outstanding electrochemical performances for Li-ion, Li-sulfur and Li-oxygen batteries. Furthermore, Hu et al. [19] proposed another strategy to address the interfacial challenges of garnet-type solid electrolytes through the deposition of an ultrathin layer of Al_2O_3 onto the surface of the garnet electrolyte using atomic layer deposition in which greatly reduced conductivity resistances from 1710 to 1 Ω cm^2 at room temperature were achieved. As a result, a full cell with $Li_2FeMn_3O_8$ (LFMO) as the cathode, garnet $Li_7La_{2.75}Ca_{0.25}Zr_{1.75}Nb_{0.25}O_{12}$ (LLCZN) as the electrolyte and Li as the anode were tested to have significant

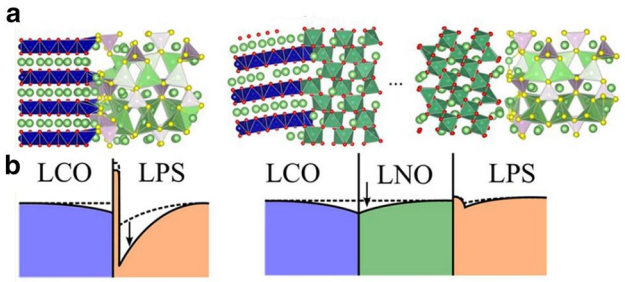

Fig. 29 **a** Schematic of the atomic structure in equilibrium and **b** Li concentration at the initial stage of charging at the interface. Reprinted with permission from Ref. [210]. Copyright 2014 American Chemical Society

improvements, which the researchers attributed to the deposited Al_2O_3 layer that can accelerate Li^+ transfer, prevent electrolyte decomposition and strengthen contact between the electrolyte and Li metal.

Li dendrites can also form along the grain boundaries in $Li_7La_3Zr_2O_{12}$ (LLZ) solid electrolytes as detected by TEM, EELS and MAS NMR, resulting in the short-circuiting of batteries. To address this, Tsai et al. [201] proposed that the reason for this dendrite growth can be the inhomogeneous contact at the interface through carefully polishing and modifying the surface with thin Au layers. Here, the researchers reported that as a result, surface contact was greatly enhanced and resistances reduced, with growth of Li dendrites being prevented at the same current densities. However, these researchers also reported that Li dendrites still appeared at higher current densities, indicating that more comprehensive and in-depth research is required. Furthermore, many new reports have been published to address interfacial engineering on LLZO [27, 202–207].

Sulfide electrolytes can also be made into all-solid-state batteries and have also attracted much attention recently [208, 209]. For example, Yao et al. [208] studied the intimate contact at the solid electrolyte–cathode interface using an in situ liquid-phase method and suggested that the $Li_7P_3S_{11}$ electrolyte particles were directly anchored onto cobalt sulfide nanosheets to lead to excellent cycling and rate performances.

5.2.2 Interface Between the Electrolyte and the Cathode

The prominent issue of interfaces between electrolytes and cathodes is instability as caused by mutual diffusion, side reaction, etc., as well as the space-charge layer effect. And similar to the solutions of anode interfaces, the introduction of buffer layers into interfaces is also effective. For example, Haruyama et al. [210] built up a buffer layer of $LiNbO_3$ (LNO) between an oxide cathode ($LiCoO_2$ (LCO)) and a sulfide electrolyte (β-Li_3PS_4 (LPS)) in an all-solid-state Li-ion conductor and through theoretical calculations of the 3 interfaces (Fig. 29), elucidated the matching structures with atomic levels and electronic properties in the interfacial regions. Here, the researchers found that the introduction of LNO layers can alleviate structural disorder at the interface, balance Li distribution and suppress growth of SCLs to boost Li conduction.

Interfacial reactions of solid electrolytes with anode and cathode materials can also affect performance [211]. For example, Auvergniot et al. [212] studied the interfacial phenomenon of argyrodite Li_6PS_5Cl toward $LiCoO_2$, $LiNi_{1/3}Co_{1/3}Mn_{1/3}O_2$ and $LiMn_2O_4$ electrodes using Auger electron spectroscopy and X-ray photoelectron spectroscopy and found that the electrolyte can be oxidized into sulfur, lithium polysulfides, P_2S_x, phosphates and LiCl at the interface. Wenzel et al. [213, 214] also investigated the interfacial zone between $Li_7P_3S_{11}$ and Li metal using in situ photoelectron spectroscopy and discovered the existence of a non-growing resistive interphase in contact with Li metal analogous to an SEI film. Similar approaches were also taken to study the interface between LLTO and Li electrodes and showed the reduction in Ti ions and Ti metal.

Overall, the introduction of buffer layers between solid electrolytes and electrodes is an effective method to control interfacial resistance. However, these artificial layers can also increase conduction resistance at the interface. Therefore, search for novel interfacial materials and synthesis of thinner deposition layers is a major direction for future development [215].

6 Conclusions and Perspectives

With the rapid progress of solid-state Li-based batteries in recent years, numerous efforts have been devoted among academic and industrial communities to enhance the performance of solid-state electrolytes. However, compared with commercial liquid electrolytes, numerous challenges need to be addressed before large-scale application. These challenges include methods to enhance Li-ion transport in the bulk, decrease grain boundary resistance at the interface between solid electrolytes and electrodes and enhance the stability of the structure and the interface of solid-state electrolytes during long term cycling (Fig. 30).

Currently, although some material systems with relatively high conductivities as Li-ion conductors have been reported, more efforts are required. And through numerous investigations, researchers have found that anion arrangements can determine the intrinsic ionic conductivity of materials in which the body-centered cubic (bbc) anion framework is proposed to be the most desirable for fast ion diffusion and low activation energy (*E*a). In addition, substitution with optimal-sized ions for a given material has extensively

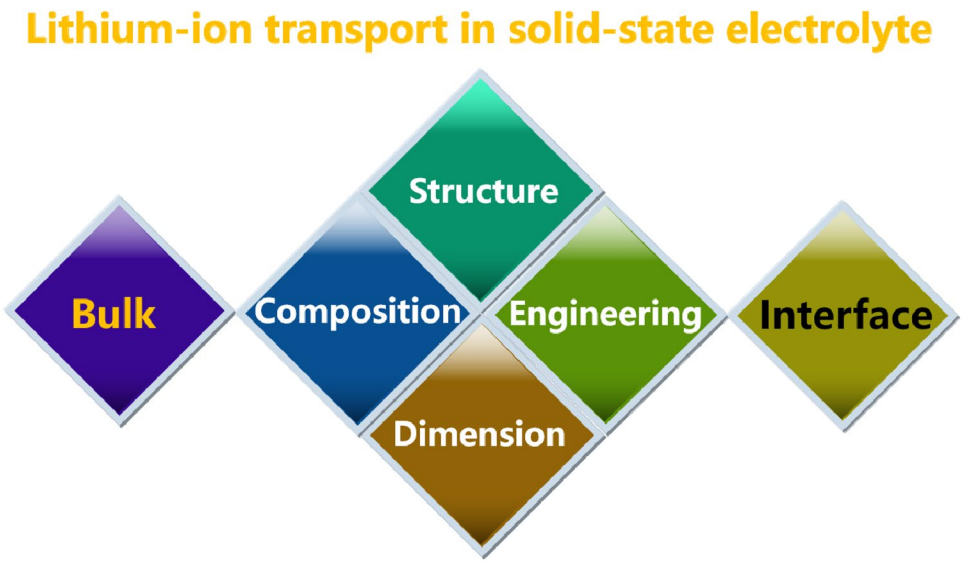

Fig. 30 Challenges and perspectives of lithium-ion transport in solid-state electrolyte

proven to be effective in the enhancement of conductivity for LISICON, NASICON, perovskite and other families by orders of magnitude in which activation energy can be reduced through expanded lattice volumes and enlarged bottleneck sizes. Aside from ionic sizes and lattice volumes, the introduction of amorphous glass into crystalline electrolytes can also enhance conductivity through so-called "composite electrolytes" or "heterogeneous electrolytes". Moreover, more intensive defects and space-charge layer effects can also contribute to improved conductivity.

Aside from Li diffusion in the bulk of solid-state electrolytes, interfacial properties also play a crucial role in the performance of all-solid-state electrolytes in which for practical applications of all-solid-state batteries, the interface between solid-state electrolytes and electrodes needs to be stable and electrochemically compatible to minimize interfacial resistances. In addition, different from liquid electrolytes, the contact at solid/solid interfaces is often insufficient. To address this, many sustainable solutions have been demonstrated to improve battery performance. For example, various surface engineering treatments can be carried out to deposit thin layers of metals, oxides and semiconductors to modify the electrolyte/electrode interface. Moreover, the polishing of electrolyte surfaces and the exerting of appropriate pressures can also be effective. More intimate contact and much smaller resistance can also be obtained through the introduction of additional soft polymer interlayers. In addition, the design and fabrication of artificial buffer layers into electrolyte/electrode interfaces can enable intimate contact to suppress side reactions and reduce transfer resistance.

Overall, future studies into solid-state electrolytes should focus on the design of multi-component nanoscale interfaces and the minimization of surface coating thicknesses. In addition, the understanding of Li-ion transport in the bulk and the interface of solid-state electrolytes through advanced characterization techniques is fundamental to the future advancement of solid-state electrolytes and can provide new perspectives into the design of high-capacity solid-state batteries.

Acknowledgements This work was supported by the National Key Research and Development Program of China (2016YFB0100203), the National Natural Science Foundation of China (U1801251, 21633003, 21673116 and 51801104), the Natural Science Foundation of Jiangsu Province of China (BK20170726), the China Postdoctoral Science Foundation (2018M632284), the Fundamental Research Funds for the Central Universities (KJQN201945), the Shanghai Pujiang Program (18PJ1403800), the Young Eastern Scholar Program of the Shanghai Municipal Education Commission and the PAPD of Jiangsu Higher Education Institutions.

References

1. Hao, M.L., Li, J., Park, S., et al.: Efficient thermal management of Li-ion batteries with a passive interfacial thermal regulator based on a shape memory alloy. Nat. Energy **3**, 899–906 (2018). https://doi.org/10.1038/s41560-018-0243-8
2. Luo, J.Y., Cui, W.J., He, P., et al.: Raising the cycling stability of aqueous lithium-ion batteries by eliminating oxygen in the electrolyte. Nat. Chem. **2**, 760–765 (2010). https://doi.org/10.1038/nchem.763
3. Wang, Y.G., Yi, J., Xia, Y.Y.: Recent progress in aqueous lithium-ion batteries. Adv. Energy Mater. **2**, 830–840 (2012). https://doi.org/10.1002/aenm.201200065

4. Xu, K.: Electrolytes and interphases in Li-ion batteries and beyond. Chem. Rev. **114**, 11503–11618 (2014). https://doi.org/10.1021/cr500003w
5. Xing, L.D., Zheng, X.W., Schroeder, M., et al.: Deciphering the ethylene carbonate–propylene carbonate mystery in Li-ion batteries. Acc. Chem. Res. **51**, 282–289 (2018). https://doi.org/10.1021/acs.accounts.7b00474
6. Xing, L.D., Li, W.S., Wang, C.Y., et al.: Theoretical investigations on oxidative stability of solvents and oxidative decomposition mechanism of ethylene carbonate for lithium ion battery use. J. Phys. Chem. B **113**, 16596–16602 (2009). https://doi.org/10.1021/jp9074064
7. Fan, W., Zhang, R.E., Wang, Z.F., et al.: Facile fabrication of polyether sulfone (PES) protecting layer on Cu foil for stable Li metal anode. Electrochim. Acta **260**, 407–412 (2018). https://doi.org/10.1016/j.electacta.2017.12.085
8. Liao, K.M., Wu, S.C., Mu, X.W., et al.: Developing a "Water-defendable" and "Dendrite-free" lithium-metal anode using a simple and promising $GeCl_4$ pretreatment method. Adv. Mater. **30**, 1705711 (2018). https://doi.org/10.1002/adma.201705711
9. Cheng, X.B., Yan, C., Peng, H.J., et al.: Sulfurized solid electrolyte interphases with a rapid Li + diffusion on dendrite-free Li metal anodes. Energy Storage Mater. **10**, 199–205 (2018). https://doi.org/10.1016/j.ensm.2017.03.008
10. Liao, B., Hu, X.L., Xu, M.Q., et al.: Constructing unique cathode interface by manipulating functional groups of electrolyte additive for graphite/$LiNi_{0.6}Co_{0.2}Mn_{0.2}O_2$ cells at high voltage. J. Phys. Chem. Lett. **9**, 3434–3445 (2018). https://doi.org/10.1021/acs.jpclett.8b01099
11. Wang, F., Borodin, O., Ding, M.S., et al.: Hybrid aqueous/non-aqueous electrolyte for safe and high-energy Li-ion batteries. Joule **2**, 927–937 (2018). https://doi.org/10.1016/j.joule.2018.02.011
12. Wang, F., Suo, L.M., Liang, Y.J., et al.: Spinel $LiNi_{0.5}Mn_{1.5}O_4$ cathode for high-energy aqueous lithium-ion batteries. Adv. Energy Mater. **7**, 1600922 (2017). https://doi.org/10.1002/aenm.201600922
13. Yang, Q.F., Li, C.L.: Li metal batteries and solid state batteries benefiting from halogen-based strategies. Energy Storage Mater. **14**, 100–117 (2018). https://doi.org/10.1016/j.ensm.2018.02.017
14. Zhang, Z.H., Zhao, Y.R., Chen, S.J., et al.: An advanced construction strategy of all-solid-state lithium batteries with excellent interfacial compatibility and ultralong cycle life. J. Mater. Chem. A **5**, 16984–16993 (2017). https://doi.org/10.1039/c7ta04320a
15. Yi, J., Guo, S.H., He, P., et al.: Status and prospects of polymer electrolytes for solid-state Li–O_2 (air) batteries. Energy Environ. Sci. **10**, 860–884 (2017). https://doi.org/10.1039/c6ee03499c
16. Yi, J., Wu, S.C., Bai, S.Y., et al.: Interfacial construction of Li_2O_2 for a performance-improved polymer Li–O_2 battery. J. Mater. Chem. A **4**, 2403–2407 (2016). https://doi.org/10.1039/c5ta10436j
17. Yi, J., Zhou, H.S.: A unique hybrid quasi-solid-state electrolyte for Li–O_2 batteries with improved cycle life and safety. Chemsuschem **9**, 2391–2396 (2016). https://doi.org/10.1002/cssc.201600536
18. Yi, J., Liu, Y., Qiao, Y., et al.: Boosting the cycle life of Li–O_2 batteries at elevated temperature by employing a hybrid polymer–ceramic solid electrolyte. ACS Energy Lett. **2**, 1378–1384 (2017). https://doi.org/10.1021/acsenergylett.7b00292
19. Han, X., Gong, Y., Fu, K., et al.: Negating interfacial impedance in garnet-based solid-state Li metal batteries. Nat. Mater. **16**, 572–579 (2017). https://doi.org/10.1038/nmat4821
20. Gao, Z.H., Sun, H.B., Fu, L., et al.: All-solid-state batteries: promises, challenges, and recent progress of inorganic solid-state electrolytes for all-solid-state lithium batteries (adv. mater. 17/2018). Adv. Mater. **30**, 1870122 (2018). https://doi.org/10.1002/adma.201870122
21. Guo, Z.Y., Li, C., Liu, J.Y., et al.: A long-life lithium-air battery in ambient air with a polymer electrolyte containing a redox mediator. Angew. Chem. Int. Ed. **56**, 7505–7509 (2017). https://doi.org/10.1002/anie.201701290
22. Guo, Z.Y., Li, J.L., Xia, Y., et al.: A flexible polymer-based Li–air battery using a reduced graphene oxide/Li composite anode. J. Mater. Chem. A **6**, 6022–6032 (2018). https://doi.org/10.1039/c8ta01117f
23. Zhang, Z.Z., Shao, Y.J., Lotsch, B., et al.: New horizons for inorganic solid state ion conductors. Energy Environ. Sci. **11**, 1945–1976 (2018). https://doi.org/10.1039/c8ee01053f
24. Takada, K.: Progress in solid electrolytes toward realizing solid-state lithium batteries. J. Power Sources **394**, 74–85 (2018). https://doi.org/10.1016/j.jpowsour.2018.05.003
25. Yue, L.P., Ma, J., Zhang, J.J., et al.: All solid-state polymer electrolytes for high-performance lithium ion batteries. Energy Storage Mater. **5**, 139–164 (2016). https://doi.org/10.1016/j.ensm.2016.07.003
26. Gao, J., Zhao, Y.S., Shi, S.Q., et al.: Lithium-ion transport in inorganic solid state electrolyte. Chin. Phys. B **25**, 018211 (2016). https://doi.org/10.1088/1674-1056/25/1/018211
27. Park, K., Yu, B.C., Jung, J.W., et al.: Electrochemical nature of the cathode interface for a solid-state lithium-ion battery: interface between $LiCoO_2$ and garnet-$Li_7La_3Zr_2O_{12}$. Chem. Mater. **28**, 8051–8059 (2016). https://doi.org/10.1021/acs.chemmater.6b03870
28. Romanenko, K., Jin, L.Y., Howlett, P., et al.: In situ MRI of operating solid-state lithium metal cells based on ionic plastic crystal electrolytes. Chem. Mater. **28**, 2844–2851 (2016). https://doi.org/10.1021/acs.chemmater.6b00797
29. Vinod Chandran, C., Pristat, S., Witt, E., et al.: Solid-state NMR investigations on the structure and dynamics of the ionic conductor $Li_{1+x}AlxTi_{2-x}(PO4)_3$ ($0.0 \le x \le 1.0$). J. Phys. Chem. C **120**, 8436–8442 (2016). https://doi.org/10.1021/acs.jpcc.6b00318
30. Bohnke, O.: Mechanism of ionic conduction and electrochemical intercalation of lithium into the perovskite lanthanum lithium titanate. Solid State Ionics **91**, 21–31 (1996). https://doi.org/10.1016/s0167-2738(96)00434-1
31. Yashima, M., Itoh, M., Inaguma, Y., et al.: Crystal structure and diffusion path in the fast lithium-ion conductor $La_{0.62}Li_{0.16}TiO_3$. J. Am. Chem. Soc. **127**, 3491–3495 (2005). https://doi.org/10.1021/ja0449224
32. Zhao, Y.S., Daemen, L.L.: Superionic conductivity in lithium-rich anti-perovskites. J. Am. Chem. Soc. **134**, 15042–15047 (2012). https://doi.org/10.1021/ja305709z
33. Zhang, Y., Zhao, Y.S., Chen, C.F.: Ab initiostudy of the stabilities of and mechanism of superionic transport in lithium-rich antiperovskites. Phys. Rev. B **87**, 134303 (2013). https://doi.org/10.1103/physrevb.87.134303
34. Braga, M.H., Ferreira, J.A., Stockhausen, V., et al.: Novel Li_3ClO based glasses with superionic properties for lithium batteries. J. Mater. Chem. A **2**, 5470–5480 (2014). https://doi.org/10.1039/c3ta15087a
35. Aono, H.: The electrical properties of ceramic electrolytes for $LiM_xTi_{2-x}(PO_4)_3$+yLi_2O, M = Ge, Sn, Hf, and Zr systems. J. Electrochem. Soc. **140**(7), 1827 (1993). https://doi.org/10.1149/1.2220723
36. Giarola, M., Sanson, A., Tietz, F., et al.: Structure and vibrational dynamics of NASICON-type $LiTi_2(PO4)_3$. J. Phys. Chem. C **121**, 3697–3706 (2017). https://doi.org/10.1021/acs.jpcc.6b11067
37. Kahlaoui, R., Arbi, K., Sobrados, I., et al.: Cation miscibility and lithium mobility in NASICON $Li_{1+x}Ti_{2-x}Sc_x(PO4)_3$ ($0 \le x \le 0.5$) series: a combined NMR and impedance study. Inorg. Chem. **56**,

1216–1224 (2017). https://doi.org/10.1021/acs.inorgchem.6b02274
38. Thangadurai, V., Kaack, H., Weppner, W.J.F.: Novel fast lithium ion conduction in garnet-type $Li_5La_3M_2O_{12}$ (M = Nb, Ta). J. Am. Ceram. Soc. **86**, 437–440 (2003). https://doi.org/10.1111/j.1151-2916.2003.tb03318.x
39. Hyooma, H., Hayashi, K.: Crystal structures of $La_3Li_5M_2O_{12}$ (M = Nb, Ta). Mater. Res. Bull. **23**, 1399–1407 (1988). https://doi.org/10.1016/0025-5408(88)90264-4
40. Thangadurai, V., Weppner, W.: Effect of sintering on the ionic conductivity of garnet-related structure $Li_5La_3Nb_2O_{12}$ and In- and K-doped $Li_5La_3Nb_2O_{12}$. J. Solid State Chem. **179**, 974–984 (2006). https://doi.org/10.1016/j.jssc.2005.12.025
41. Thangadurai, V., Weppner, W.: Li6ALa$_2$Nb$_2$O$_{12}$ (A = Ca, Sr, Ba): a new class of fast lithium ion conductors with garnet-like structure. J. Am. Ceram. Soc. **88**, 411–418 (2005). https://doi.org/10.1111/j.1551-2916.2005.00060.x
42. Thangadurai, V., Weppner, W.: Li6ALa$_2$Ta$_2$O$_{12}$ (A = Sr, Ba): novel garnet-like oxides for fast lithium ion conduction. Adv. Funct. Mater. **15**, 107–112 (2005). https://doi.org/10.1002/adfm.200400044
43. Narayanan, S., Ramezanipour, F., Thangadurai, V.: Enhancing Li ion conductivity of garnet-type $Li_5La_3Nb_2O_{12}$ by Y- and Li-codoping: synthesis, structure, chemical stability, and transport properties. J. Phys. Chem. C **116**, 20154–20162 (2012). https://doi.org/10.1021/jp304737x
44. Murugan, R., Thangadurai, V., Weppner, W.: Fast lithium ion conduction in garnet-type $Li_7La_3Zr_2O_{12}$. Angew. Chem. Int. Ed. **46**, 7778–7781 (2007). https://doi.org/10.1002/anie.200701144
45. Jalem, R., Yamamoto, Y., Shiiba, H., et al.: Concerted migration mechanism in the Li ion dynamics of garnet-type $Li_7La_3Zr_2O_{12}$. Chem. Mater. **25**, 425–430 (2013). https://doi.org/10.1021/cm303542x
46. Awaka, J., Kijima, N., Hayakawa, H., et al.: Synthesis and structure analysis of tetragonal $Li_7La_3Zr_2O_{12}$ with the garnet-related type structure. J. Solid State Chem. **182**, 2046–2052 (2009). https://doi.org/10.1016/j.jssc.2009.05.020
47. Awaka, J., Takashima, A., Kataoka, K., et al.: Crystal structure of fast lithium-ion-conducting cubic $Li_7La_3Zr_2O_{12}$. Chem. Lett. **40**, 60–62 (2011). https://doi.org/10.1246/cl.2011.60
48. Rangasamy, E., Wolfenstine, J., Sakamoto, J.: The role of Al and Li concentration on the formation of cubic garnet solid electrolyte of nominal composition $Li_7La_3Zr_2O_{12}$. Solid State Ionics **206**, 28–32 (2012). https://doi.org/10.1016/j.ssi.2011.10.022
49. Thangadurai, V., Adams, S., Weppner, W.: Crystal structure revision and identification of Li^+-ion migration pathways in the garnet-like $Li_5La_3M_2O_{12}$(M = Nb, Ta) oxides. Chem. Mater. **16**, 2998–3006 (2004). https://doi.org/10.1021/cm031176d
50. Cussen, E.J.: The structure of lithium garnets: cation disorder and clustering in a new family of fast Li^+ conductors. Chem. Commun. **4**, 412–413 (2006). https://doi.org/10.1039/b514640b
51. van Wüllen, L., Echelmeyer, T., Meyer, H.W., et al.: The mechanism of Li-ion transport in the garnet $Li_5La_3Nb_2O_{12}$. Phys. Chem. Chem. Phys. **9**, 3298–3303 (2007). https://doi.org/10.1039/b703179c
52. Xu, M., Park, M.S., Lee, J.M., et al.: Mechanisms of Li^+ transport in garnet-type cubic $Li_{3+x}La_3M_2O_{12}$ (M = Te, Nb, Zr). Phys. Rev. B **85**, 052301 (2012). https://doi.org/10.1103/physrevb.85.052301
53. Kanno, R.: Synthesis of a new lithium ionic conductor, thio-LISICON–lithium germanium sulfide system. Solid State Ionics **130**, 97–104 (2000). https://doi.org/10.1016/s0167-2738(00)00277-0
54. Kanno, R., Murayama, M.: Lithium ionic conductor thio-LISICON: the Li_2S-GeS_2-P_2S_5 system. J. Electrochem. Soc. **148**, A472–A476 (2001)
55. Kamaya, N., Homma, K., Yamakawa, Y., et al.: A lithium superionic conductor. Nat. Mater. **10**, 682–686 (2011). https://doi.org/10.1038/nmat3066
56. Du, F.M., Ren, X.D., Yang, J., et al.: Structures, thermodynamics, and li$^+$ mobility of $Li_{10}GeP_2S_{12}$: a first-principles analysis. J. Phys. Chem. C **118**, 10590–10595 (2014). https://doi.org/10.1021/jp5000039
57. Xu, M., Ding, J., Ma, E.: One-dimensional stringlike cooperative migration of lithium ions in an ultrafast ionic conductor. Appl. Phys. Lett. **101**, 031901 (2012). https://doi.org/10.1063/1.4737397
58. Wenzel, S., Randau, S., Leichtweiß, T., et al.: Direct observation of the interfacial instability of the fast ionic conductor $Li_{10}GeP_2S_{12}$ at the lithium metal anode. Chem. Mater. **28**, 2400–2407 (2016). https://doi.org/10.1021/acs.chemmater.6b00610
59. Kuhn, A., Duppel, V., Lotsch, B.V.: Tetragonal $Li_{10}GeP_2S_{12}$ and Li_7GePS_8-exploring the Li ion dynamics in LGPS Li electrolytes. Energy Environ. Sci. **6**, 3548 (2013). https://doi.org/10.1039/c3ee41728j
60. Bron, P., Johansson, S., Zick, K., et al.: $Li_{10}SnP_2S_{12}$: an affordable lithium superionic conductor. J. Am. Chem. Soc. **135**, 15694–15697 (2013). https://doi.org/10.1021/ja407393y
61. Sun, Y.L., Suzuki, K., Hori, S., et al.: Superionic conductors: $Li_{10+\delta}[Sn_ySi_{1-y}]_{1+\delta}P_{2-\delta}S_{12}$ with a $Li_{10}GeP_2S_{12}$-type structure in the Li_3PS_4-Li_4SnS_4-Li_4SiS_4 quasi-ternary system. Chem. Mater. **29**, 5858–5864 (2017). https://doi.org/10.1021/acs.chemmater.7b00886
62. Kuhn, A., Gerbig, O., Zhu, C.B., et al.: A new ultrafast superionic Li-conductor: ion dynamics in $Li_{11}Si_2PS_{12}$ and comparison with other tetragonal LGPS-type electrolytes. Phys. Chem. Chem. Phys. **16**, 14669–14674 (2014). https://doi.org/10.1039/c4cp02046d
63. Kato, Y., Hori, S., Saito, T., et al.: High-power all-solid-state batteries using sulfide superionic conductors. Nat. Energy **1**, 16030 (2016). https://doi.org/10.1038/nenergy.2016.30
64. Krauskopf, T., Culver, S.P., Zeier, W.G.: Bottleneck of diffusion and inductive effects in Li10Ge$_{1-x}$Sn$_x$P$_2$S$_{12}$. Chem. Mater. **30**, 1791–1798 (2018). https://doi.org/10.1021/acs.chemmater.8b00266
65. Deiseroth, H.J., Kong, S.T., Eckert, H., et al.: Li_6PS_5X: a class of crystalline Li-rich solids with an unusually high Li^+ mobility. Angew. Chem. Int. Ed. **47**, 755–758 (2008). https://doi.org/10.1002/anie.200703900
66. Kraft, M.A., Culver, S.P., Calderon, M., et al.: Influence of lattice polarizability on the ionic conductivity in the lithium superionic argyrodites Li_6PS_5X (X = Cl, Br, I). J. Am. Chem. Soc. **139**, 10909–10918 (2017). https://doi.org/10.1021/jacs.7b06327
67. de Klerk, N.J.J., Rosłoń, I., Wagemaker, M.: Diffusion mechanism of Li argyrodite solid electrolytes for Li-ion batteries and prediction of optimized halogen doping: the effect of Li vacancies, halogens, and halogen disorder. Chem. Mater. **28**, 7955–7963 (2016). https://doi.org/10.1021/acs.chemmater.6b03630
68. Sicolo, S., Kalcher, C., Sedlmaier, S.J., et al.: Diffusion mechanism in the superionic conductor Li_4PS_4I studied by first-principles calculations. Solid State Ionics **319**, 83–91 (2018). https://doi.org/10.1016/j.ssi.2018.01.046
69. Minafra, N., Culver, S.P., Krauskopf, T., et al.: Effect of Si substitution on the structural and transport properties of superionic Li-argyrodites. J. Mater. Chem. A **6**, 645–651 (2018). https://doi.org/10.1039/c7ta08581h
70. Richards, W.D., Wang, Y., Miara, L.J., et al.: Design of $Li_{1+2x}Zn_{1-x}PS_4$, a new lithium ion conductor. Energy Environ. Sci. **9**, 3272–3278 (2016). https://doi.org/10.1039/c6ee02094a

71. Kaup, K., Lalère, F., Huq, A., et al.: Correlation of structure and fast ion conductivity in the solid solution series $Li_{1+2x}Zn_{1-x}PS_4$. Chem. Mater. **30**, 592–596 (2018). https://doi.org/10.1021/acs.chemmater.7b05108
72. Wang, Y., Richards, W.D., Ong, S.P., et al.: Design principles for solid-state lithium superionic conductors. Nat. Mater. **14**, 1026–1031 (2015)
73. Kuhn, A., Holzmann, T., Nuss, J., et al.: A facile wet chemistry approach towards unilamellar tin sulfide nanosheets from $Li_{4x}Sn_{1-x}S_2$ solid solutions. J. Mater. Chem. A **2**, 6100–6106 (2014). https://doi.org/10.1039/c3ta14190j
74. Brant, J.A., Massi, D.M., Holzwarth, N.A.W., et al.: Fast lithium ion conduction in Li_2SnS_3: synthesis, physicochemical characterization, and electronic structure. Chem. Mater. **27**, 189–196 (2015). https://doi.org/10.1021/cm5037524
75. Holzmann, T., Schoop, L.M., Ali, M.N., et al.: $Li_{0.6}[Li_{0.2}Sn_{0.8}S_2]$-a layered lithium superionic conductor. Energy Environ. Sci. **9**, 2578–2585 (2016). https://doi.org/10.1039/c6ee00633g
76. Fenton, D.E., Parker, J.M., Wright, P.V.: Complexes of alkali metal ions with poly(ethylene oxide). Polymer **14**, 589 (1973). https://doi.org/10.1016/0032-3861(73)90146-8
77. Abraham, K.M.: Li^+-conductive solid polymer electrolytes with liquid-like conductivity. J. Electrochem. Soc. **137**, 1657 (1990). https://doi.org/10.1149/1.2086749
78. Ahmad, S.: Polymer electrolytes: characteristics and peculiarities. Ionics **15**, 309–321 (2009)
79. Meyer, W.H.: Polymer electrolytes for lithium-ion batteries. Adv. Mater. **10**, 439–448 (1998)
80. Golodnitsky, D., Strauss, E., Peled, E., et al.: Review: on order and disorder in polymer electrolytes. J. Electrochem. Soc. **162**, A2551–A2566 (2015). https://doi.org/10.1149/2.0161514jes
81. Wright, P.V.: Polymer electrolytes: the early days. Electrochim. Acta **43**, 1137–1143 (1998). https://doi.org/10.1016/s0013-4686(97)10011-1
82. Fullerton-Shirey, S.K., Maranas, J.K.: Effect of $LiClO_4$ on the structure and mobility of PEO-based solid polymer electrolytes. Macromolecules **42**, 2142–2156 (2009). https://doi.org/10.1021/ma802502u
83. Quartarone, E.: PEO-based composite polymer electrolytes. Solid State Ionics **110**, 1–14 (1998). https://doi.org/10.1016/s0167-2738(98)00114-3
84. Bruce, P.G., Vincent, C.A.: Polymer electrolytes. Faraday Trans. **89**, 3187–3203 (1993). https://doi.org/10.1039/ft9938903187
85. Bouchet, R., Maria, S., Meziane, R., et al.: Single-ion BAB triblock copolymers as highly efficient electrolytes for lithium-metal batteries. Nat. Mater. **12**, 452–457 (2013)
86. Angell, C.A., Liu, C., Sanchez, E.: Rubbery solid electrolytes with dominant cationic transport and high ambient conductivity. Nature **362**, 137–139 (1993). https://doi.org/10.1038/362137a0
87. Croce, F., Appetecchi, G.B., Persi, L., et al.: Nanocomposite polymer electrolytes for lithium batteries. Nature **394**, 456–458 (1998). https://doi.org/10.1038/28818
88. Lin, D.C., Liu, W., Liu, Y.Y., et al.: High ionic conductivity of composite solid polymer electrolyte via in situ synthesis of monodispersed SiO_2 nanospheres in poly(ethylene oxide). Nano Lett. **16**, 459–465 (2016). https://doi.org/10.1021/acs.nanolett.5b04117
89. Kumar, B., Scanlon, L.G., Spry, R.J.: On the origin of conductivity enhancement in polymer-ceramic composite electrolytes. J. Power Sources **96**, 337–342 (2001). https://doi.org/10.1016/s0378-7753(00)00665-0
90. Kumar, B., Rodrigues, S.J., Scanlon, L.G.: Ionic conductivity of polymer-ceramic composites. J. Electrochem. Soc. **148**, A1191–A1195 (2001). https://doi.org/10.1149/1.1403729
91. Ahn, J.H., Wang, G.X., Liu, H.K., et al.: Nanoparticle-dispersed PEO polymer electrolytes for Li batteries. J. Power Sources **119–121**, 422–426 (2003). https://doi.org/10.1016/s0378-7753(03)00264-7
92. Kumar, B., Scanlon, L., Marsh, R., et al.: Structural evolution and conductivity of PEO: $LiBF_4$–MgO composite electrolytes. Electrochim. Acta **46**, 1515–1521 (2001). https://doi.org/10.1016/s0013-4686(00)00747-7
93. Ramesh, S., Winie, T., Arof, A.K.: Investigation of mechanical properties of polyvinyl chloride-polyethylene oxide (PVC-PEO) based polymer electrolytes for lithium polymer cells. Eur. Polym. J. **43**, 1963–1968 (2007). https://doi.org/10.1016/j.eurpolymj.2007.02.006
94. Xi, J.Y., Qiu, X.P., Li, J., et al.: PVDF–PEO blends based microporous polymer electrolyte: effect of PEO on pore configurations and ionic conductivity. J. Power Sources **157**, 501–506 (2006). https://doi.org/10.1016/j.jpowsour.2005.08.009
95. Sengwa, R.J., Dhatarwal, P., Choudhary, S.: Role of preparation methods on the structural and dielectric properties of plasticized polymer blend electrolytes: correlation between ionic conductivity and dielectric parameters. Electrochim. Acta **142**, 359–370 (2014). https://doi.org/10.1016/j.electacta.2014.07.120
96. Wen, Z.Y., Itoh, T., Ichikawa, Y., et al.: Blend-based polymer electrolytes of poly(ethylene oxide) and hyperbranched poly[bis(triethylene glycol)benzoate] with terminal acetyl groups. Solid State Ionics **134**, 281–289 (2000). https://doi.org/10.1016/S0167-2738(00)00707-4
97. Rolland, J., Brassinne, J., Bourgeois, J.P., et al.: Chemically anchored liquid-PEO based block copolymer electrolytes for solid-state lithium-ion batteries. J. Mater. Chem. A **2**, 11839–11846 (2014). https://doi.org/10.1039/c4ta02327g
98. Yuan, F., Chen, H.Z., Yang, H.Y., et al.: PAN–PEO solid polymer electrolytes with high ionic conductivity. Mater. Chem. Phys. **89**, 390–394 (2005). https://doi.org/10.1016/j.matchemphys.2004.09.032
99. Chaker, J.A., Santilli, C.V., Pulcinelli, S.H., et al.: Multi-scale structural description of siloxane: PPO hybrid ionic conductors doped by sodium salts. J. Mater. Chem. **17**, 744–757 (2007). https://doi.org/10.1039/b612587e
100. Acosta, J.L., Morales, E.: Structural, morphological and electrical characterization of polymer electrolytes based on PEO/PPO blends. Solid State Ionics **85**, 85–90 (1996). https://doi.org/10.1016/0167-2738(96)00045-8
101. Chen, C.L., Chang, T.W., Su, S.C., et al.: High performance solid-state dye-sensitized solar cells based on poly(acrylonitrile-co-vinyl acetate)/TiO_2 nanoparticles redox electrolytes. J. Power Sources **247**, 406–411 (2014). https://doi.org/10.1016/j.jpowsour.2013.08.117
102. Zhang, S.S., Xu, K., Jow, T.R.: Li-ion cell with poly(acrylonitrile-methyl methacrylate)-based gel polymer electrolyte. Solid State Ionics **158**, 375–380 (2003). https://doi.org/10.1016/s0167-2738(02)00914-1
103. Zhang, S.S., Jow, T.R.: Study of poly(acrylonitrile-methyl methacrylate) as binder for graphite anode and $LiMn_2O_4$ cathode of Li-ion batteries. J. Power Sources **109**, 422–426 (2002). https://doi.org/10.1016/S0378-7753(02)00107-6
104. Sugimoto, H., Inoue, S.: Copolymerization of carbon dioxide and epoxide. J. Polym. Sci. A Polym. Chem. **42**, 5561–5573 (2004). https://doi.org/10.1002/pola.20319
105. Zhang, J.J., Yang, J.F., Dong, T.T., et al.: Aliphatic polycarbonate-based solid-state polymer electrolytes for advanced lithium batteries: advances and perspective. Small **14**, 1800821 (2018). https://doi.org/10.1002/smll.201800821

106. Borghini, M.C.: Electrochemical properties of polyethylene oxide-Li[$(CF_3SO_2)_2N$]-Gamma-$LiAlO_2$ composite polymer electrolytes. J. Electrochem. Soc. **142**, 2118–2121 (1995). https://doi.org/10.1149/1.2044260
107. Kimura, K., Motomatsu, J., Tominaga, Y.: Highly concentrated polycarbonate-based solid polymer electrolytes having extraordinary electrochemical stability. J. Polym. Sci. B Polym. Phys. **54**, 2442–2447 (2016). https://doi.org/10.1002/polb.24235
108. Okumura, T., Nishimura, S.: Lithium ion conductive properties of aliphatic polycarbonate. Solid State Ionics **267**, 68–73 (2014). https://doi.org/10.1016/j.ssi.2014.09.011
109. Zhang, Z.H., Shi, Q., Peng, J., et al.: Partial delamination of the organo-montmorillonite with surfactant containing hydroxyl groups in maleated poly(propylene carbonate). Polymer **47**, 8548–8555 (2006). https://doi.org/10.1016/j.polymer.2006.09.041
110. Inoue, S., Koinuma, H., Tsuruta, T.: Copolymerization of carbon dioxide and epoxide with organometallic compounds. Die Makromolekulare Chemie **130**, 210–220 (1969). https://doi.org/10.1002/macp.1969.021300112
111. Mang, S., Cooper, A.I., Colclough, M.E., et al.: Copolymerization of CO_2 and 1,2-cyclohexene oxide using a CO_2-soluble chromium porphyrin catalyst. Macromolecules **33**, 303–308 (2000). https://doi.org/10.1021/ma991162m
112. Zhou, L., He, J.H., Zhang, J., et al.: Facile in situ synthesis of manganese dioxide nanosheets on cellulose fibers and their application in oxidative decomposition of formaldehyde. J. Phys. Chem. C **115**, 16873–16878 (2011). https://doi.org/10.1021/jp2050564
113. Wang, Z.H., Chien, W.C., Yue, T.W., et al.: Application of heparinized cellulose affinity membranes in recombinant adeno-associated virus serotype 2 binding and delivery. J. Membr. Sci. **310**, 141–148 (2008). https://doi.org/10.1016/j.memsci.2007.10.048
114. Jackson, E.L., Hudson, C.S.: Application of the cleavage type of oxidation by periodic acid to starch and cellulose. J. Am. Chem. Soc. **59**, 2049–2050 (1937). https://doi.org/10.1021/ja01289a077
115. Zhang, J.J., Liu, Z.H., Kong, Q.S., et al.: Renewable and superior thermal-resistant cellulose-based composite nonwoven as lithium-ion battery separator. ACS Appl. Mater. Interfaces. **5**, 128–134 (2013). https://doi.org/10.1021/am302290n
116. Zhang, J.J., Zhao, J.H., Yue, L.P., et al.: Safety-reinforced poly(propylene carbonate)-based all-solid-state polymer electrolyte for ambient-temperature solid polymer lithium batteries. Adv. Energy Mater. **5**, 1501082 (2015). https://doi.org/10.1002/aenm.201501082
117. Sun, B., Mindemark, J., Edström, K., et al.: Polycarbonate-based solid polymer electrolytes for Li-ion batteries. Solid State Ionics **262**, 738–742 (2014). https://doi.org/10.1016/j.ssi.2013.08.014
118. Kang, Y.K., Lee, J., Suh, D.H., et al.: A new polysiloxane based cross-linker for solid polymer electrolyte. J. Power Sources **146**, 391–396 (2005). https://doi.org/10.1016/j.jpowsour.2005.03.142
119. Zhang, Z.C., Sherlock, D., West, R., et al.: Cross-linked network polymer electrolytes based on a polysiloxane backbone with oligo(oxyethylene) side chains: synthesis and conductivity. Macromolecules **36**, 9176–9180 (2003). https://doi.org/10.1021/ma0349276
120. Grünebaum, M., Hiller, M.M., Jankowsky, S., et al.: Synthesis and electrochemistry of polymer based electrolytes forlithium batteries. Prog. Solid State Chem. **42**, 85–105 (2014)
121. Oh, B., Vissers, D., Zhang, Z., et al.: New interpenetrating network type poly(siloxane-g-ethylene oxide) polymer electrolyte for lithium battery. J. Power Sources **119–121**, 442–447 (2003). https://doi.org/10.1016/S0378-7753(03)00187-3
122. Fonseca, C.P., Neves, S.: Characterization of polymer electrolytes based on poly(dimethyl siloxane-co-ethylene oxide). J. Power Sources **104**, 85–89 (2002). https://doi.org/10.1016/S0378-7753(01)00902-8
123. Hooper, R., Lyons, L.J., Mapes, M.K., et al.: Highly conductive siloxane polymers. Macromolecules **34**, 931–936 (2001). https://doi.org/10.1021/ma0018446
124. Whitfield, P.S., Abouimrane, A., Davidson, I.J.: In-situ XRD study of the succinonitrile–lithium bis(trifluoromethylsulfonyl) imide (LiTFSI) phase diagram. Solid State Ionics **181**, 740–744 (2010). https://doi.org/10.1016/j.ssi.2010.04.004
125. Alarco, P.J., Abu-Lebdeh, Y., Abouimrane, A., et al.: The plastic-crystalline phase of succinonitrile as a universal matrix for solid-state ionic conductors. Nat. Mater. **3**, 476–481 (2004). https://doi.org/10.1038/nmat1158
126. Long, S.: Fast ion conduction in molecular plastic crystals. Solid State Ionics **161**, 105–112 (2003). https://doi.org/10.1016/s0167-2738(03)00208-x
127. Ha, H.J., Kwon, Y.H., Kim, J.Y., et al.: A self-standing, UV-cured polymer networks-reinforced plastic crystal composite electrolyte for a lithium-ion battery. Electrochim. Acta **57**, 40–45 (2011). https://doi.org/10.1016/j.electacta.2011.03.101
128. Fan, L.Z., Maier, J.: Composite effects in poly(ethylene oxide)-succinonitrile based all-solid electrolytes. Electrochem. Commun. **8**, 1753–1756 (2006). https://doi.org/10.1016/j.elecom.2006.08.017
129. Fan, L.Z., Hu, Y.S., Bhattacharyya, A., et al.: Su as a versatile additive for polymer electrolytes. Adv. Funct. Mater. **17**, 2800–2807 (2007). https://doi.org/10.1002/adfm.200601070
130. Ha, H.J., Kil, E.H., Kwon, Y.H., et al.: UV-curable semi-interpenetrating polymer network-integrated, highly bendable plastic crystal composite electrolytes for shape-conformable all-solid-state lithium ion batteries. Energy Environ. Sci. **5**, 6491–6499 (2012). https://doi.org/10.1039/c2ee03025j
131. Tambelli, C.C., Bloise, A.C., Rosário, A.V., et al.: Characterisation of PEO–Al_2O_3 composite polymer electrolytes. Electrochim. Acta **47**, 1677–1682 (2002). https://doi.org/10.1016/s0013-4686(01)00900-8
132. Sun, H.Y., Takeda, Y., Imanishi, N., et al.: Ferroelectric materials as a ceramic filler in solid composite polyethylene oxide-based electrolytes. J. Electrochem. Soc. **147**, 2462–2467 (2000). https://doi.org/10.1149/1.1393554
133. Croce, F., Persi, L., Scrosati, B., et al.: Role of the ceramic fillers in enhancing the transport properties of composite polymer electrolytes. Electrochim. Acta **46**, 2457–2461 (2001). https://doi.org/10.1016/s0013-4686(01)00458-3
134. Bronstein, L.M., Karlinsey, R.L., Ritter, K., et al.: Design of organic–inorganic solid polymer electrolytes: synthesis, structure, and properties. J. Mater. Chem. **14**, 1812–1820 (2004). https://doi.org/10.1039/b401826e
135. Adebahr, J., Byrne, N., Forsyth, M., et al.: Enhancement of ion dynamics in PMMA-based gels with addition of TiO_2 nanoparticles. Electrochim. Acta **48**, 2099–2103 (2003). https://doi.org/10.1016/s0013-4686(03)00191-9
136. Kumar, B.: From colloidal to composite electrolytes: properties, peculiarities, and possibilities. J. Power Sources **135**, 215–231 (2004). https://doi.org/10.1016/j.jpowsour.2004.04.038
137. Appetecchi, G.B., Passerini, S.: PEO-carbon composite lithium polymer electrolyte. Electrochim. Acta **45**, 2139–2145 (2000). https://doi.org/10.1016/s0013-4686(99)00437-5
138. Michael, M.S., Jacob, M.M.E., Prabaharan, S.R.S., et al.: Enhanced lithium ion transport in PEO-based solid polymer electrolytes employing a novel class of plasticizers. Solid State Ionics **98**, 167–174 (1997). https://doi.org/10.1016/s0167-2738(97)00117-3

139. Croce, F., Curini, R., Martinelli, A., et al.: Physical and chemical properties of nanocomposite polymer electrolytes. J. Phys. Chem. B **74**, 1008–1025 (1999)
140. Liang, C.C.: Conduction characteristics of the lithium iodide-aluminum oxide solid electrolytes. J. Electrochem. Soc. **120**, 1289 (1973). https://doi.org/10.1149/1.2403248
141. Croce, F.: Nanocomposite polymer electrolytes and their impact on the lithium battery technology. Solid State Ionics **135**, 47–52 (2000). https://doi.org/10.1016/s0167-2738(00)00329-5
142. Shanmukaraj, D., Murugan, R.: Characterization of PEG: $LiClO_4 + SrBi_4Ti_4O_{15}$ nanocomposite polymer electrolytes for lithium secondary batteries. J. Power Sources **149**, 90–95 (2005). https://doi.org/10.1016/j.jpowsour.2005.02.008
143. Scrosati, B., Croce, F., Persi, L.: Impedance spectroscopy study of PEO-based nanocomposite polymer electrolytes. J. Electrochem. Soc. **147**, 1718 (2000). https://doi.org/10.1149/1.1393423
144. Lin, C.W., Hung, C.L., Venkateswarlu, M., et al.: Influence of TiO_2 nano-particles on the transport properties of composite polymer electrolyte for lithium-ion batteries. J. Power Sources **146**, 397–401 (2005). https://doi.org/10.1016/j.jpowsour.2005.03.028
145. Yeh, J.M., Liou, S.J., Lin, C.Y., et al.: Anticorrosively enhanced PMMA–clay nanocomposite materials with quaternary alkylphosphonium salt as an intercalating agent. Chem. Mater. **14**, 154–161 (2002). https://doi.org/10.1021/cm010337f
146. Zhang, Y.G., Zhao, Y., Gosselink, D., et al.: Synthesis of poly(ethylene-oxide)/nanoclay solid polymer electrolyte for all solid-state lithium/sulfur battery. Ionics **21**, 381–385 (2015). https://doi.org/10.1007/s11581-014-1176-2
147. Coleman, J.N., Khan, U., Blau, W.J., et al.: Small but strong: a review of the mechanical properties of carbon nanotube–polymer composites. Carbon **44**, 1624–1652 (2006). https://doi.org/10.1016/j.carbon.2006.02.038
148. Udomvech, A., Kerdcharoen, T., Osotchan, T.: First principles study of Li and Li + adsorbed on carbon nanotube: variation of tubule diameter and length. Chem. Phys. Lett. **406**, 161–166 (2005). https://doi.org/10.1016/j.cplett.2005.02.084
149. Tang, C.Y., Hackenberg, K., Fu, Q., et al.: High ion conducting polymer nanocomposite electrolytes using hybrid nanofillers. Nano Lett. **12**, 1152–1156 (2012). https://doi.org/10.1021/nl202692y
150. Knauth, P.: Inorganic solid Li ion conductors: an overview. Solid State Ionics **180**, 911–916 (2009). https://doi.org/10.1016/j.ssi.2009.03.022
151. Choi, J.H., Lee, C.H., Yu, J.H., et al.: Enhancement of ionic conductivity of composite membranes for all-solid-state lithium rechargeable batteries incorporating tetragonal $Li_7La_3Zr_2O_{12}$ into a polyethylene oxide matrix. J. Power Sources **274**, 458–463 (2015). https://doi.org/10.1016/j.jpowsour.2014.10.078
152. Xu, K.: Nonaqueous liquid electrolytes for lithium-based rechargeable batteries. Chem. Rev. **104**, 4303–4418 (2004). https://doi.org/10.1021/cr030203g
153. Zhang, B.K., Tan, R., Yang, L.Y., et al.: Mechanisms and properties of ion-transport in inorganic solid electrolytes. Energy Storage Mater. **10**, 139–159 (2018). https://doi.org/10.1016/j.ensm.2017.08.015
154. van der Ven, A., Bhattacharya, J., Belak, A.A.: Understanding Li diffusion in Li-intercalation compounds. Acc. Chem. Res. **46**, 1216–1225 (2013). https://doi.org/10.1021/ar200329r
155. Souquet, J.L.: Ionic transport in amorphous solid electrolytes. Annu. Rev. Mater. Sci. **11**, 211–231 (1981). https://doi.org/10.1146/annurev.ms.11.080181.001235
156. Berthier, L., Biroli, G.: Theoretical perspective on the glass transition and amorphous materials. Rev. Mod. Phys. **83**, 587–645 (2011). https://doi.org/10.1103/revmodphys.83.587
157. Ratner, M.A., Shriver, D.F.: Ion transport in solvent-free polymers. Chem. Rev. **88**, 109–124 (1988). https://doi.org/10.1021/cr00083a006
158. Dawar, A., Chandra, A.: Electric field driven fractal growth in polymer electrolyte composites: experimental evidence of theoretical simulations. Phys. Lett. A **376**, 3604–3608 (2012). https://doi.org/10.1016/j.physleta.2012.10.034
159. Wagemaker, M., Kearley, G.J., van Well, A.A., et al.: Multiple Li positions inside oxygen octahedra in lithiated TiO_2 Anatase. J. Am. Chem. Soc. **125**, 840–848 (2003). https://doi.org/10.1021/ja028165q
160. Wieczorek, W.: Composite polyether based solid electrolytes: the Lewis acid-base approach. Solid State Ionics **85**, 67–72 (1996). https://doi.org/10.1016/0167-2738(96)00042-2
161. Liu, Q.H., Peng, B., Shen, M., et al.: Polymer chain diffusion and Li^+ hopping of poly(ethylene oxide)/$LiAsF_6$ crystalline polymer electrolytes as studied by solid state NMR and ac impedance. Solid State Ionics **255**, 74–79 (2014). https://doi.org/10.1016/j.ssi.2013.11.053
162. Maier, J.: Ionic conduction in space charge regions. Prog. Solid State Ch. **23**, 171–263 (1995). https://doi.org/10.1016/0079-6786(95)00004-e
163. Khandkar, A.: The system AgI-AgBr: energetic consequences of defect equilibria in single-phase and two-phase regions. J. Electrochem. Soc. **131**, 2683 (1984). https://doi.org/10.1149/1.2115383
164. Maier, J.: Defect chemistry in heterogeneous systems. Solid State Ionics **75**, 139–145 (1995). https://doi.org/10.1016/0167-2738(94)00222-e
165. Maier, J.: Space-charge regions in solid 2-phase systems and their conduction contribution. 3. Defect chemistry and ionic conductivity in thin films. Solid State Ionics **23**, 59–67 (1987). https://doi.org/10.1016/0167-2738(87)90082-8
166. Maier, J.: Size effects on mass transport and storage in lithium batteries. J. Power Sources **174**, 569–574 (2007). https://doi.org/10.1016/j.jpowsour.2007.06.246
167. Maekawa, H.: Size-dependent ionic conductivity observed for ordered mesoporous alumina-LiI composite. Solid State Ionics **175**, 281–285 (2004). https://doi.org/10.1016/j.ssi.2003.12.032
168. Maekawa, H., Iwatani, T., Shen, H.Y., et al.: Enhanced lithium ion conduction and the size effect on interfacial phase in Li_2ZnI_4–mesoporous alumina composite electrolyte. Solid State Ionics **178**, 1637–1641 (2008). https://doi.org/10.1016/j.ssi.2007.10.018
169. Maier, J.: Nanoionics: ion transport and electrochemical storage in confined systems. Nat. Mater. **4**, 805–815 (2005). https://doi.org/10.1038/nmat1513
170. Arbi, K., Bucheli, W., Jiménez, R., et al.: High lithium ion conducting solid electrolytes based on NASICON $Li_{1+x}Al_xM_{2-x}(PO_4)_3$ materials (M = Ti, Ge and $0 \le x \le 0.5$). J. Eur. Ceram. Soc. **35**, 1477–1484 (2015). https://doi.org/10.1016/j.jeurceramsoc.2014.11.023
171. Wang, D.W., Zhong, G.M., Pang, W.K., et al.: Toward understanding the lithium transport mechanism in garnet-type solid electrolytes: Li^+ ion exchanges and their mobility at octahedral/tetrahedral sites. Chem. Mater. **27**, 6650–6659 (2015). https://doi.org/10.1021/acs.chemmater.5b02429
172. Liang, X.M., Wang, L.Y., Jiang, Y.M., et al.: In-channel and in-plane Li ion diffusions in the superionic conductor $Li_{10}GeP_2S_{12}$ probed by solid-state NMR. Chem. Mater. **27**, 5503–5510 (2015). https://doi.org/10.1021/acs.chemmater.5b01384
173. Xiang, Y.X., Zheng, G.R., Zhong, G.M., et al.: Toward understanding of ion dynamics in highly conductive lithium ion conductors: some perspectives by solid state NMR techniques. Solid State Ionics **318**, 19–26 (2018). https://doi.org/10.1016/j.ssi.2017.11.025

174. Bouchard, L.S., Kovtunov, K., Burt, S., et al.: Para-hydrogen-enhanced hyperpolarized gas-phase magnetic resonance imaging. Angew. Chem. Int. Ed. **46**, 4064–4068 (2007). https://doi.org/10.1002/anie.200700830
175. Emsley, L.: Advances in magnetic resonance: from stem cells to catalytic surfaces. J. Am. Chem. Soc. **135**, 8089–8091 (2013). https://doi.org/10.1021/ja404269a
176. Wang, M.T., Feindel, K.W., Bergens, S.H., et al.: In situ quantification of the in-plane water content in the Nafion® membrane of an operating polymer-electrolyte membrane fuel cell using 1H micro-magnetic resonance imaging experiments. J. Power Sources **195**, 7316–7322 (2010). https://doi.org/10.1016/j.jpowsour.2010.05.029
177. Davenport, A.J., Forsyth, M., Britton, M.M.: Visualisation of chemical processes during corrosion of zinc using magnetic resonance imaging. Electrochem. Commun. **12**, 44–47 (2010). https://doi.org/10.1016/j.elecom.2009.10.032
178. Chandrashekar, S., Oparaji, O., Yang, G., et al.: Communication-^{7}Li MRI unveils concentration dependent diffusion in polymer electrolyte batteries. J. Electrochem. Soc. **163**, A2988–A2990 (2016). https://doi.org/10.1149/2.0681614jes
179. Chien, P.H., Feng, X.Y., Tang, M.X., et al.: Li distribution heterogeneity in solid electrolyte $Li_{10}GeP_2S_{12}$ upon electrochemical cycling probed by ^{7}Li MRI. J. Phys. Chem. Lett. **9**, 1990–1998 (2018). https://doi.org/10.1021/acs.jpclett.8b00240
180. Bachman, J.C., Muy, S., Grimaud, A., et al.: Inorganic solid-state electrolytes for lithium batteries: mechanisms and properties governing ion conduction. Chem. Rev. **116**, 140–162 (2016). https://doi.org/10.1021/acs.chemrev.5b00563
181. Xu, X.X., Wen, Z.Y., Yang, X.L., et al.: Dense nanostructured solid electrolyte with high Li-ion conductivity by spark plasma sintering technique. Mater. Res. Bull. **43**, 2334–2341 (2008). https://doi.org/10.1016/j.materresbull.2007.08.007
182. Jung, Y.S., Oh, D.Y., Nam, Y.J., et al.: Issues and challenges for bulk-type all-solid-state rechargeable lithium batteries using sulfide solid electrolytes. Isr. J. Chem. **55**, 472–485 (2015). https://doi.org/10.1002/ijch.201400112
183. Goodenough, J.B.: Oxide-ion electrolytes. Annu. Rev. Mater. Res. **33**, 91–128 (2003). https://doi.org/10.1146/annurev.matsci.33.022802.091651
184. Kim, H., Ding, Y., Kohl, P.A.: LiSICON: ionic liquid electrolyte for lithium ion battery. J. Power Sources **198**, 281–286 (2012). https://doi.org/10.1016/j.jpowsour.2011.10.005
185. Miara, L.J., Ong, S.P., Mo, Y.F., et al.: Effect of Rb and Ta doping on the ionic conductivity and stability of the garnet $Li_{7+2x-y}(La_{3-x}Rb_x)(Zr_{2-y}Ta_y)O_{12}$ ($0 \leqslant x \leqslant 0.375$, $0 \leqslant y \leqslant 1$) superionic conductor: a first principles investigation. Chem. Mater. **25**, 3048–3055 (2013). https://doi.org/10.1021/cm401232r
186. Ong, S.P., Mo, Y.F., Richards, W.D., et al.: Phase stability, electrochemical stability and ionic conductivity of the $Li_{10\,+/-\,1}MP_2X_{12}$ (M = Ge, Si, Sn, Al or P, and X = O, S or Se) family of superionic conductors. Energy Environ. Sci. **6**, 148–156 (2013). https://doi.org/10.1039/c2ee23355j
187. Kim, S., Hirayama, M., Cho, W., et al.: Low temperature synthesis and ionic conductivity of the epitaxial $Li_{0.17}La_{0.61}TiO_3$ film electrolyte. CrystEngComm **16**, 1044–1049 (2014). https://doi.org/10.1039/c3ce42003e
188. Kim, S., Hirayama, M., Suzuki, K., et al.: Hetero-epitaxial growth of $Li_{0.17}La_{0.61}TiO_3$ solid electrolyte on $LiMn_2O_4$ electrode for all solid-state batteries. Solid State Ionics **262**, 578–581 (2014). https://doi.org/10.1016/j.ssi.2013.09.040
189. Maier, J.: Space charge regions in solid two-phase systems and their conduction contribution: I: conductance enhancement in the system ionic conductor-'inert' phase and application on AgC1: Al_2O_3 and AgC1: SiO_2. J. Phys. Chem. Solids **46**, 309–320 (1985). https://doi.org/10.1016/0022-3697(85)90172-6
190. Cao, J., Wang, L., Shang, Y.M., et al.: Dispersibility of nano-TiO_2 on performance of composite polymer electrolytes for Li-ion batteries. Electrochim. Acta **111**, 674–679 (2013). https://doi.org/10.1016/j.electacta.2013.08.048
191. Bhattacharyya, A.J., Maier, J.: Second phase effects on the conductivity of non-aqueous salt solutions: "Soggy sand electrolytes". Adv. Mater. **16**, 811–814 (2004). https://doi.org/10.1002/adma.200306210
192. Kumazaki, S., Iriyama, Y., Kim, K.H., et al.: High lithium ion conductive $Li_7La_3Zr_2O_{12}$ by inclusion of both Al and Si. Electrochem. Commun. **13**, 509–512 (2011). https://doi.org/10.1016/j.elecom.2011.02.035
193. Gurevitch, I., Buonsanti, R., Teran, A.A., et al.: Nanocomposites of titanium dioxide and polystyrene-poly(ethylene oxide) block copolymer as solid-state electrolytes for lithium metal batteries. J. Electrochem. Soc. **160**, A1611–A1617 (2013). https://doi.org/10.1149/2.117309jes
194. Sumathipala, H.H., Hassoun, J., Panero, S., et al.: Li-$LiFePO_4$ rechargeable polymer battery using dual composite polymer electrolytes. J. Appl. Electrochem. **38**, 39–42 (2007). https://doi.org/10.1007/s10800-007-9395-0
195. Jadhav, H.S., Kalubarme, R.S., Jang, S.Y., et al.: B_2O_3-added lithium aluminium germanium phosphate solid electrolyte for Li–O_2 rechargeable batteries. Dalton Trans. **43**, 11723–11727 (2014). https://doi.org/10.1039/c4dt01144a
196. Kumar, B., Thomas, D., Kumar, J.: Space-charge-mediated superionic transport in lithium ion conducting glass-ceramics. J. Electrochem. Soc. **156**, A506 (2009). https://doi.org/10.1149/1.3122903
197. Thokchom, J.S., Kumar, B.: The effects of crystallization parameters on the ionic conductivity of a lithium aluminum germanium phosphate glass-ceramic. J. Power Sources **195**, 2870–2876 (2010). https://doi.org/10.1016/j.jpowsour.2009.11.037
198. Kali, R., Mukhopadhyay, A.: Spark plasma sintered/synthesized dense and nanostructured materials for solid-state Li-ion batteries: overview and perspective. J. Power Sources **247**, 920–931 (2014). https://doi.org/10.1016/j.jpowsour.2013.09.010
199. Kotobuki, M., Kanamura, K., Sato, Y., et al.: Electrochemical properties of $Li_7La_3Zr_2O_{12}$ solid electrolyte prepared in argon atmosphere. J. Power Sources **199**, 346–349 (2012). https://doi.org/10.1016/j.jpowsour.2011.10.060
200. Fu, K.K., Gong, Y.H., Liu, B.Y., et al.: Toward garnet electrolyte–based Li metal batteries: an ultrathin, highly effective, artificial solid-state electrolyte/metallic Li interface. Sci. Adv. **3**, e1601659 (2017). https://doi.org/10.1126/sciadv.1601659
201. Tsai, C.L., Roddatis, V., Chandran, C.V., et al.: $Li_7La_3Zr_2O_{12}$ interface modification for Li dendrite prevention. ACS Appl. Mater. Interfaces. **8**, 10617–10626 (2016). https://doi.org/10.1021/acsami.6b00831
202. Luo, W., Gong, Y.H., Zhu, Y.Z., et al.: Transition from superlithiophobicity to superlithiophilicity of garnet solid-state electrolyte. J. Am. Chem. Soc. **138**, 12258–12262 (2016)
203. Du, F.M., Zhao, N., Li, Y.Q., et al.: All solid state lithium batteries based on lamellar garnet-type ceramic electrolytes. J. Power Sources **300**, 24–28 (2015). https://doi.org/10.1016/j.jpowsour.2015.09.061
204. Xu, B.Y., Li, W.L., Duan, H.N., et al.: Li_3PO_4-added garnet-type $Li_{6.5}La3Zr_{1.5}Ta_{0.5}O_{12}$ for Li-dendrite suppression. J. Power Sources **354**, 68–73 (2017). https://doi.org/10.1016/j.jpowsour.2017.04.026
205. Vardar, G., Bowman, W.J., Lu, Q.Y., et al.: Structure, chemistry, and charge transfer resistance of the interface between $Li_7La_3Zr_2O_{12}$ electrolyte and $LiCoO_2$ cathode. Chem. Mater. **30**, 6259–6276 (2018). https://doi.org/10.1021/acs.chemmater.8b01713

206. Sharafi, A., Kazyak, E., Davis, A.L., et al.: Surface chemistry mechanism of ultra-low interfacial resistance in the solid-state electrolyte $Li_7La_3Zr_2O_{12}$. Chem. Mater. **29**, 7961–7968 (2017). https://doi.org/10.1021/acs.chemmater.7b03002
207. Lu, Y., Huang, X., Ruan, Y.D., et al.: An in situ element permeation constructed high endurance Li–LLZO interface at high current densities. J. Mater. Chem. A **6**, 18853–18858 (2018). https://doi.org/10.1039/c8ta07241h
208. Yao, X.Y., Liu, D., Wang, C.S., et al.: High-energy all-solid-state lithium batteries with ultralong cycle life. Nano Lett. **16**, 7148–7154 (2016). https://doi.org/10.1021/acs.nanolett.6b03448
209. Nagata, H., Chikusa, Y.: A lithium sulfur battery with high power density. J. Power Sources **264**, 206–210 (2014). https://doi.org/10.1016/j.jpowsour.2014.04.106
210. Haruyama, J., Sodeyama, K., Han, L.Y., et al.: Space–charge layer effect at interface between oxide cathode and sulfide electrolyte in all-solid-state lithium-ion battery. Chem. Mater. **26**, 4248–4255 (2014). https://doi.org/10.1021/cm5016959
211. Takada, K., Ohno, T., Ohta, N., et al.: Positive and negative aspects of interfaces in solid-state batteries. ACS Energy Lett. **3**, 98–103 (2018). https://doi.org/10.1021/acsenergylett.7b01105
212. Auvergniot, J., Cassel, A., Ledeuil, J.B., et al.: Interface stability of argyrodite Li_6PS_5Cl toward $LiCoO_2$, $LiNi_{1/3}Co_{1/3}Mn_{1/3}O_2$, and $LiMn_2O_4$ in bulk all-solid-state batteries. Chem. Mater. **29**, 3883–3890 (2017). https://doi.org/10.1021/acs.chemmater.6b04990
213. Wenzel, S., Weber, D.A., Leichtweiss, T., et al.: Interphase formation and degradation of charge transfer kinetics between a lithium metal anode and highly crystalline $Li_7P_3S_{11}$ solid electrolyte. Solid State Ionics **286**, 24–33 (2016). https://doi.org/10.1016/j.ssi.2015.11.034
214. Wenzel, S., Leichtweiss, T., Krüger, D., et al.: Interphase formation on lithium solid electrolytes: an in situ approach to study interfacial reactions by photoelectron spectroscopy. Solid State Ionics **278**, 98–105 (2015). https://doi.org/10.1016/j.ssi.2015.06.001
215. Zhou, W.D., Wang, S.F., Li, Y.T., et al.: Plating a dendrite-free lithium anode with a polymer/ceramic/polymer sandwich electrolyte. J. Am. Chem. Soc. **138**, 9385–9388 (2016). https://doi.org/10.1021/jacs.6b05341

Wenjia Zhao obtained her Ph.D. in Physical Chemistry of Materials from Zhejiang University in 2016. She is now a lecturer in Nanjing Agricultural University and works as a postdoctoral fellow at Nanjing University. Her major research interest is new types of batteries.

Jin Yi received his Ph. D. from Fudan University in 2014 and later worked as a postdoctoral researcher in National Institute of Advanced Industrial Science and Technology (AIST), Japan. Currently, he is an associate professor of Shanghai University. His research interests involve electrochemical functional materials and their application in Li(Na)-ion batteries, solid-state batteries and metal-air batteries.

Ping He was born in Nanjing, China, in 1981. He obtained his Ph. D. in Physical Chemistry from Fudan University in 2009 and later worked as a postdoctoral fellow at National Institute of Advanced Industrial Science and Technology (AIST), Japan. He currently is a Full Professor of College of Engineering and Applied Sciences at Nanjing University. His research interests focus on electrochemical functional materials and energy storage system such as lithium-ion batteries and lithium-air batteries.

Haoshen Zhou obtained his Bachelor from Nanjing University in 1985 and received his Ph.D. from the University of Tokyo in 1994. He is a prime senior researcher of National Institute of Advanced Industrial Science and Technology and a joint professor in Nanjing University. His research interest involves the energy active materials and their application in various batteries.